Mössbauer Spectroscopy

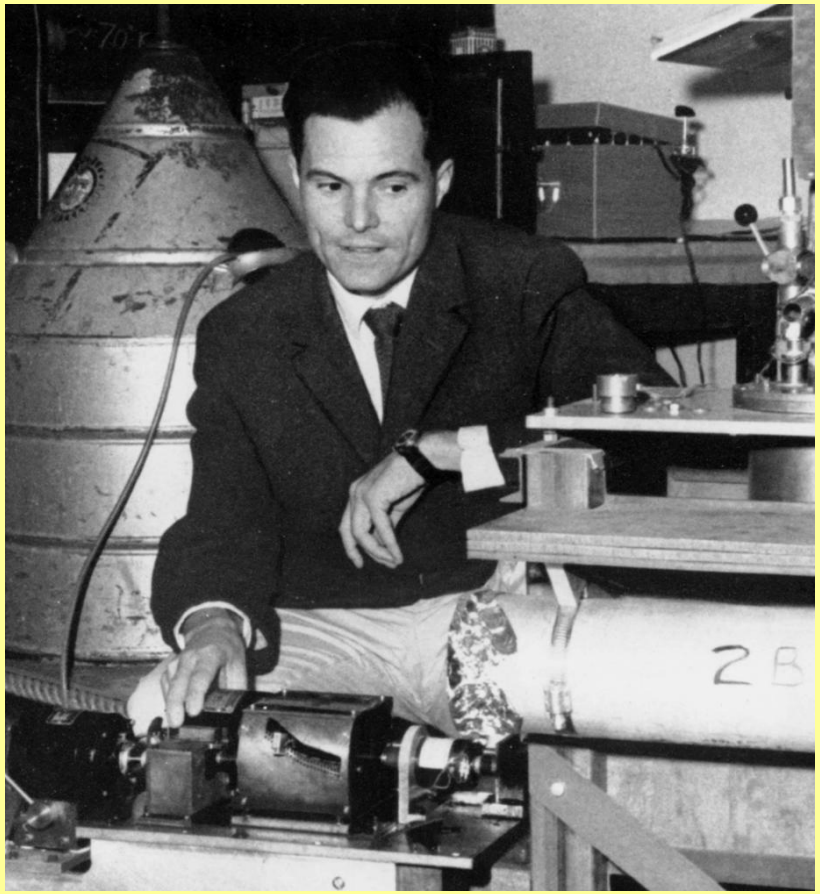

Rudolf L. Mössbauer
1929 - 2011

1958
Recoilless Nuclear Resonance Absorption of Gamma-Radiation = the Mössbauer Effect (during PhD)

1961
Nobel Prize in Physics

The Mössbauer resonance line is extremely narrow and allows hyperfine interactions to be resolved and evaluated, quadrupole splitting and an isomer shift

The Mössbauer Effect

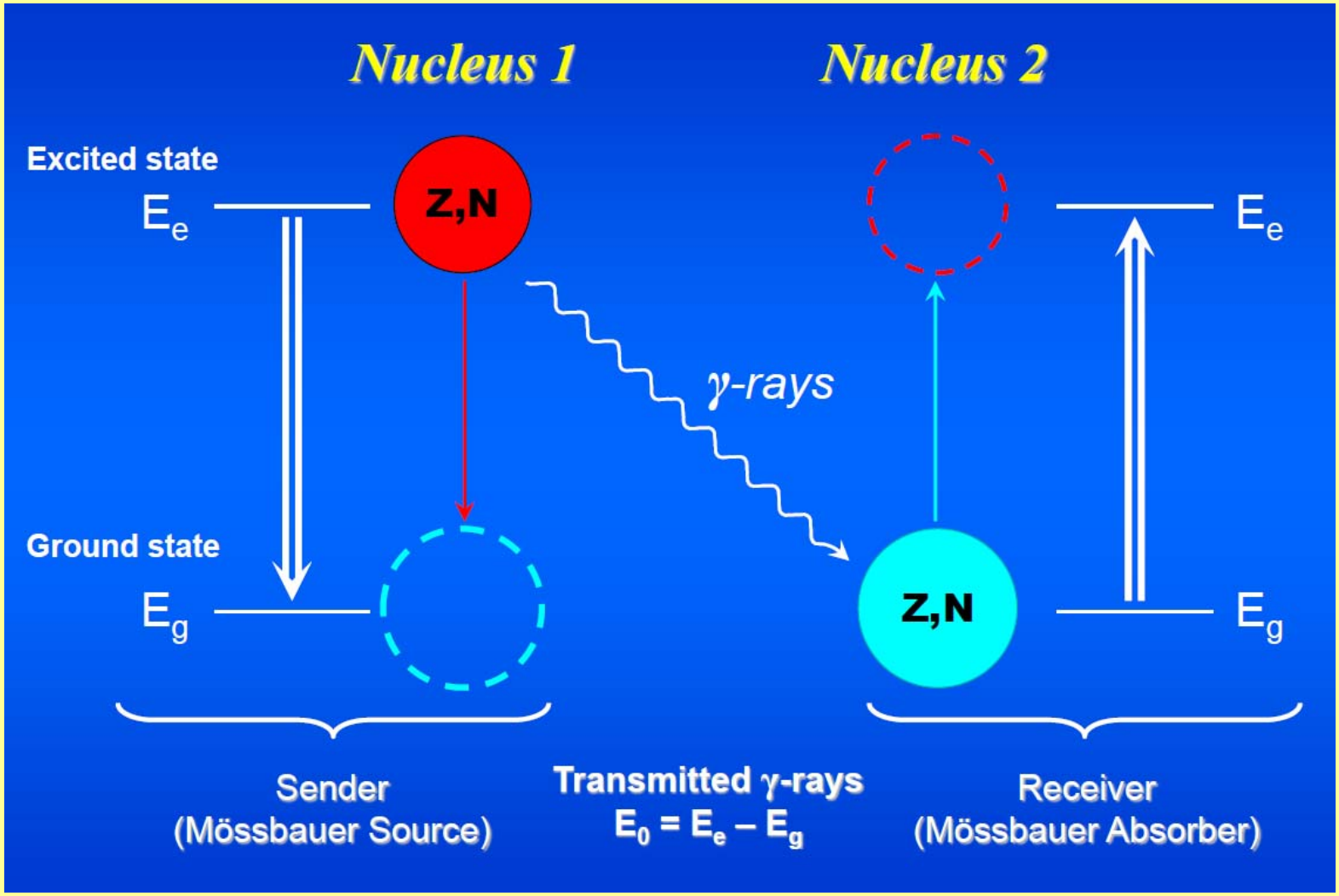

Recoilless Nuclear Resonance Absorption and Fluorescence of γ-Radiation

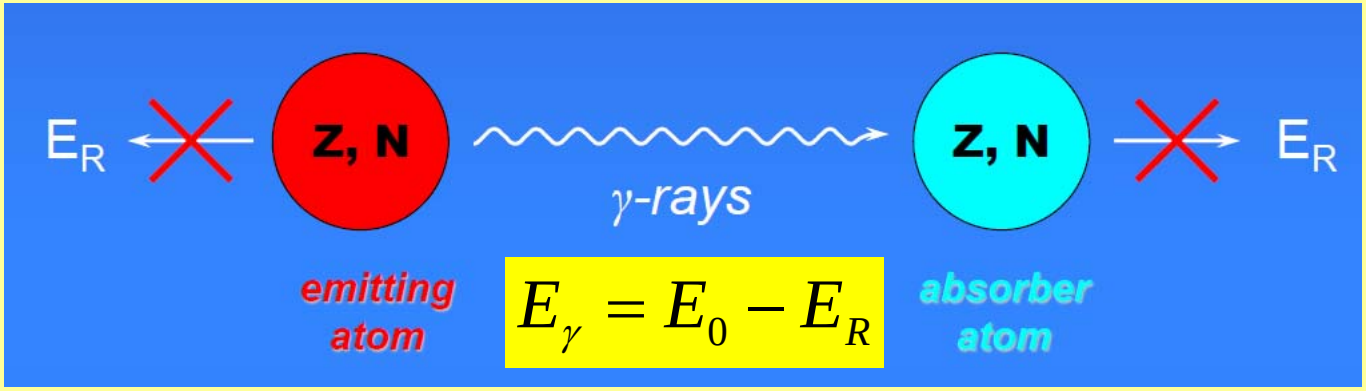

$$E_\gamma = E_0 - E_R$$

$$E_R = \frac{E_\gamma^2}{2mc^2}$$

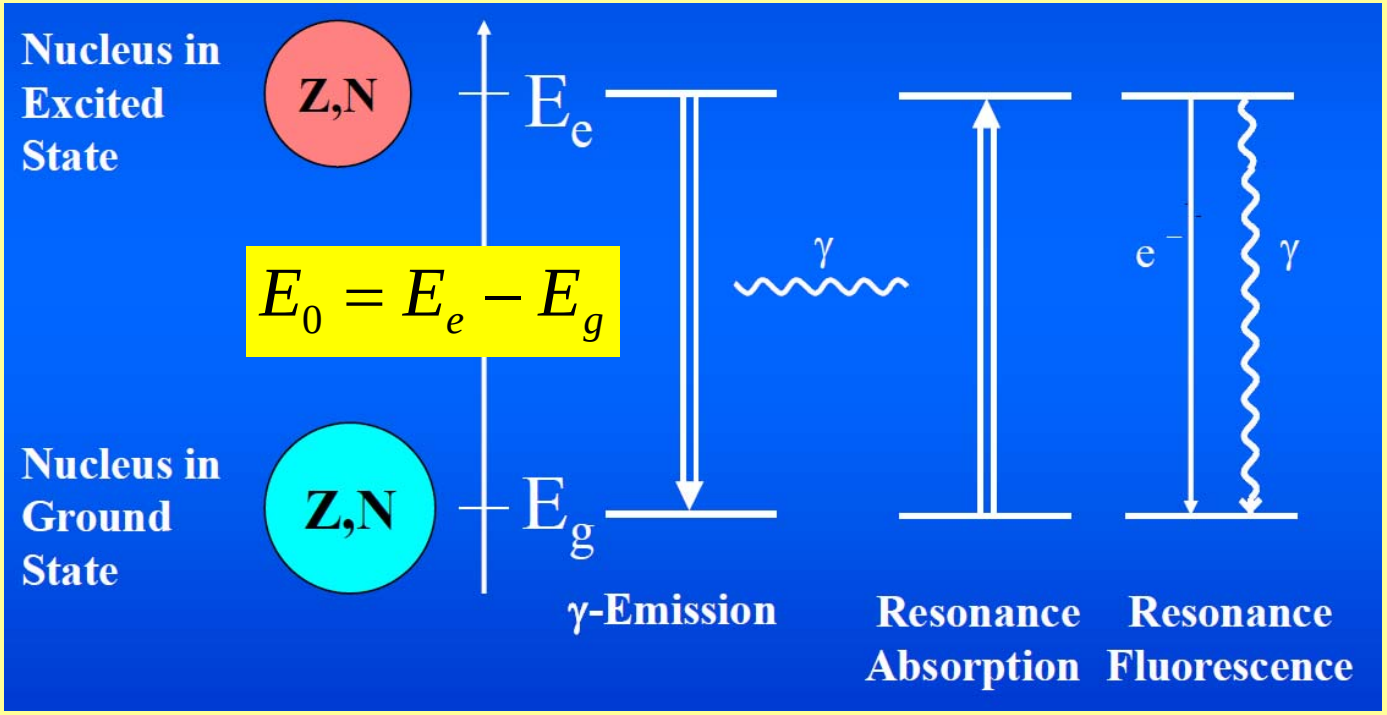

Nuclear Decay Scheme for ^{57}Fe Mössbauer Resonance

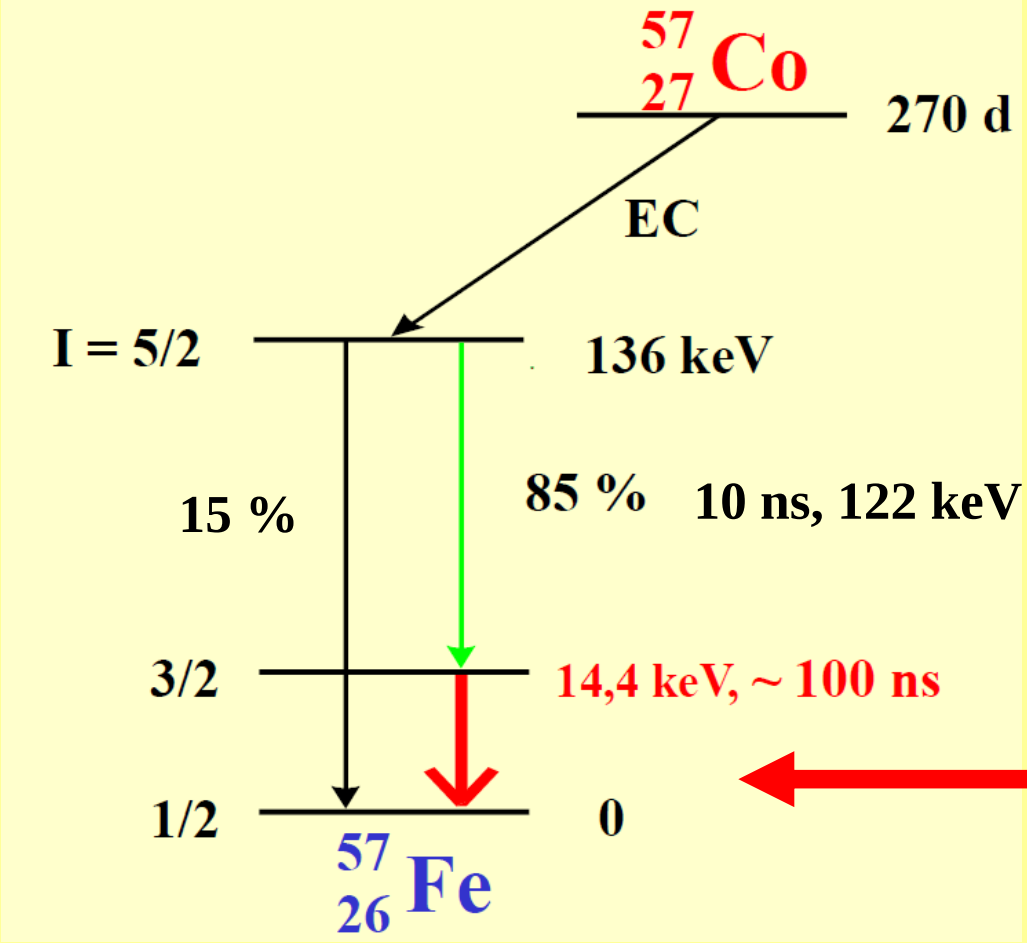

Radioactive ^{57}Co (halflife 270 d) is generated in a cyclotron and diffused into Rh

serves as the gamma radiation source for ^{57}Fe Mössbauer spectroscopy

Mössbauer Emission

Nuclear Resonance Absorption

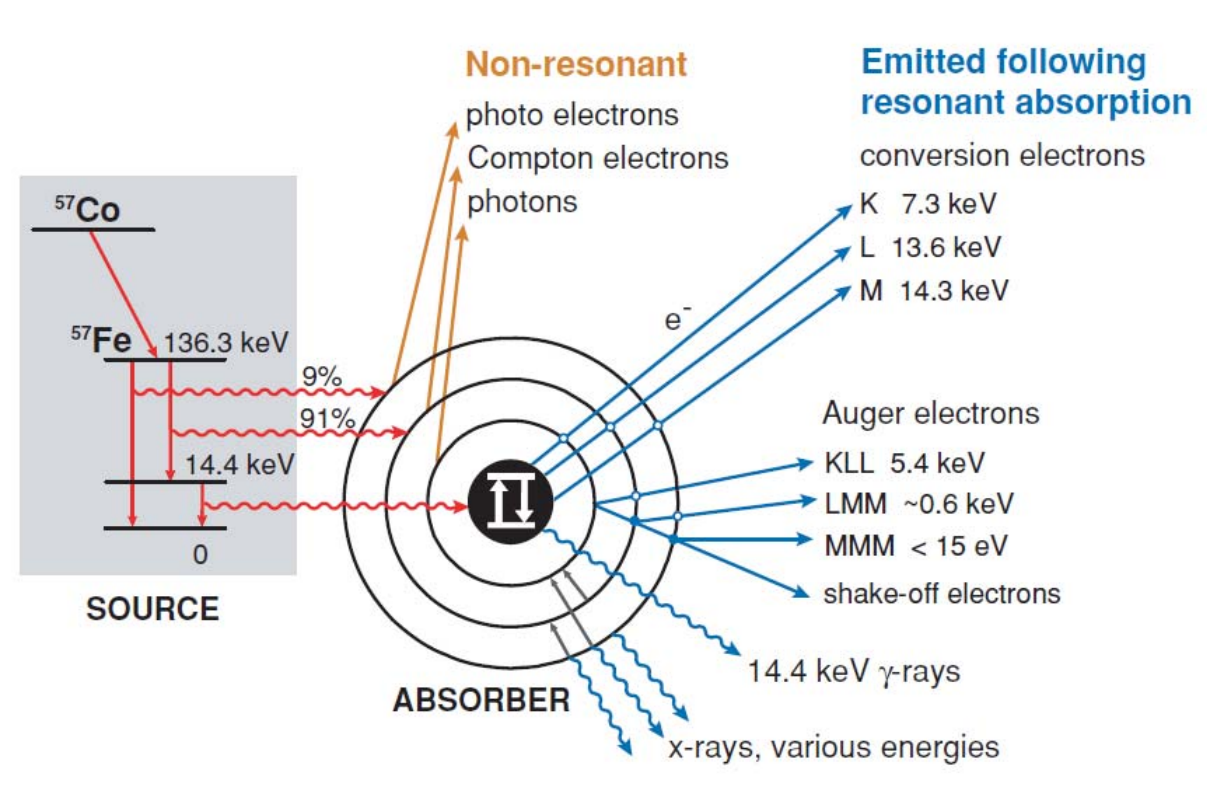

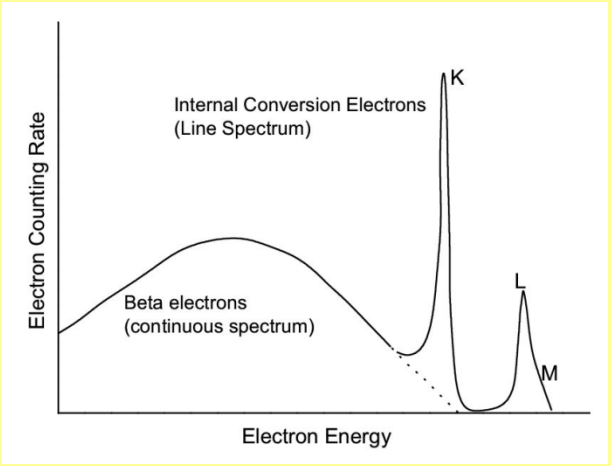

Mössbauer Active Elements

Nuclides suitable for Mössbauer spectroscopy:

Excited nuclear state lifetimes 10^{-6} - 10^{-11} s

Transition energies 5 -180 keV.

Longer (shorter) lifetimes = too narrow (broad) emission and absorption lines, no effective overlap

Transition energies > 180 keV = too large recoil, < 5 keV = absorbed in the source and absorber material

The Mössbauer effect detected in 80 isotopes of 50 elements,

only 20 elements studied in practice Fe, Sn, Sb, Te, I, Au, Ni, Ru, Ir, W, Kr, Xe, rare earth elements, Np. More than 90 % of publications refer to ^{57}Fe

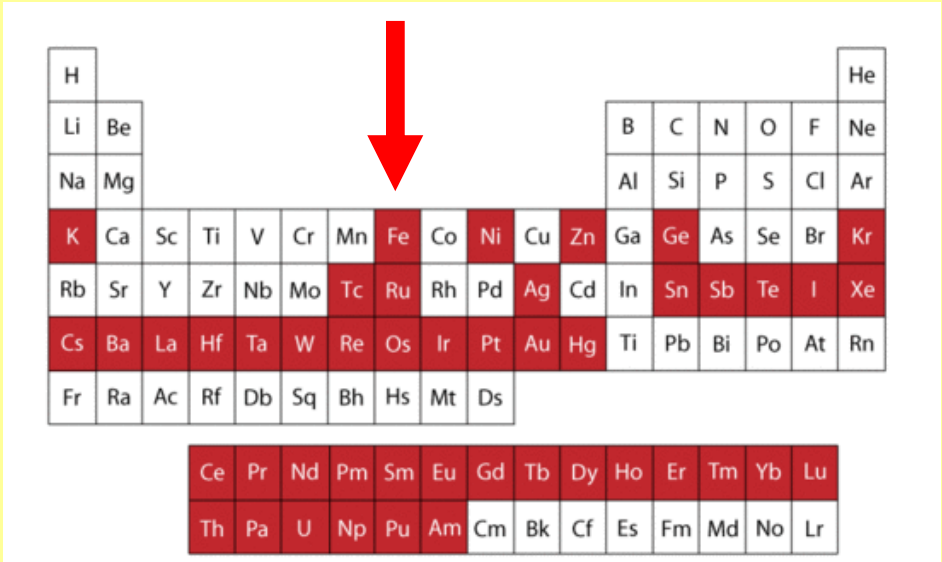

Nuclear Parameters for Selected Mössbauer Isotopes

Isotope	E_γ/keV	Γ_r/(mm s^{-1}) = 2 Γ_{nat}	I_g	I_e	α	Natural abundance %	Nuclear decay*
^{57}Fe	14.41	0.192	1/2–	3/2–	8.17	2.17	^{57}Co(EC 270 d)
^{61}Ni	67.40	0.78	3/2–	5/2–	0.12	1.25	^{61}Co(β⁻99 m)
^{119}Sn	23.87	0.626	1/2+	3/2+	5.12	8.58	^{119m}Sn(IT 50 d)
^{121}Sb	37.15	2.1	5/2+	7/2+	~10	57.25	^{121m}Sn(β⁻76 y)
^{125}Te	35.48	5.02	1/2+	3/2+	12.7	6.99	^{125}I(EC 60d)
^{127}I	57.60	2.54	5/2+	7/2+	3.70	100	^{127m}Te (β⁻109 d)
^{129}I	27.72	0.59	7/2+	5/2+	5.3	nil	^{129m}Te (β⁻33 d)
^{149}Sm	22.5	1.60	7/2–	5/2–	~12	13.9	^{149}Eu(EC 106 d)
^{151}Eu	21.6	1.44	5/2+	7/2+	29	47.8	^{151}Gd(EC 120 d)
^{161}Dy	25.65	0.37	5/2+	5/2–	~2.5	18.88	^{161}Tb(β⁻6.9 d)
^{193}Ir	73.0	0.60	3/2+	1/2+	~6	61.5	^{193}Os(β⁻31 h)
^{197}Au	77.34	1.87	3/2+	1/2+	4.0	100	^{197}Pt(β⁻18 h)
^{237}Np	59.54	0.067	5/2+	5/2–	1.06	nil	^{241}Am(α458 y)

EC = electron capture, β⁻=beta-decay, IT = isomeric transition, α = alpha-decay

Mössbauer Source

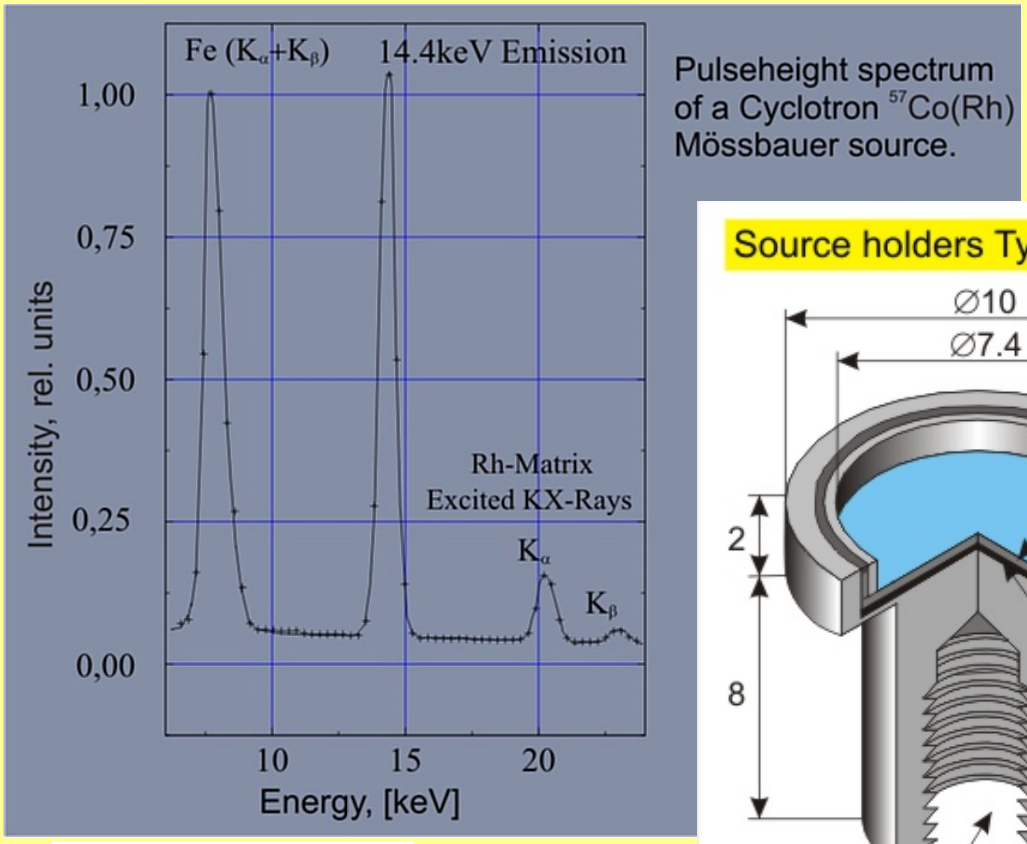

Pulseheight spectrum of a Cyclotron ^{57}Co(Rh) Mössbauer source.

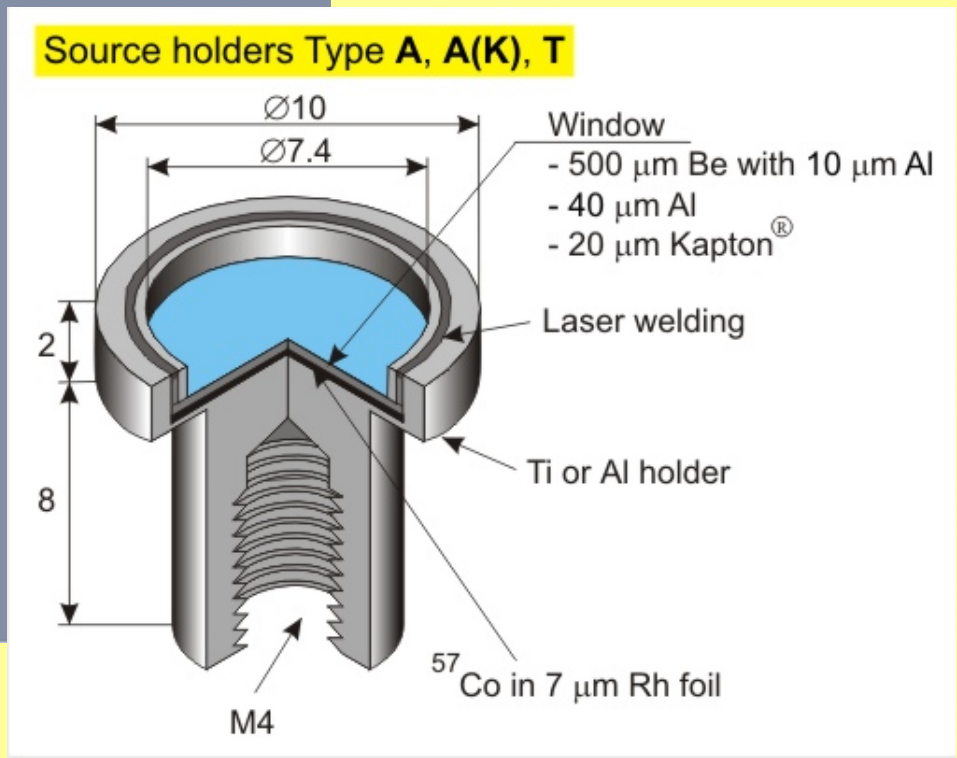

Reference Absorbers

Activity = 10 -270 mCi, lifetime 10 y

1 Ci = 37 GBq

Mössbauer Source

^{119m}Sn source = $CaSnO_3$ matrix with ^{119m}Sn
Activity = 2 - 40 mCi, lifetime 10 y

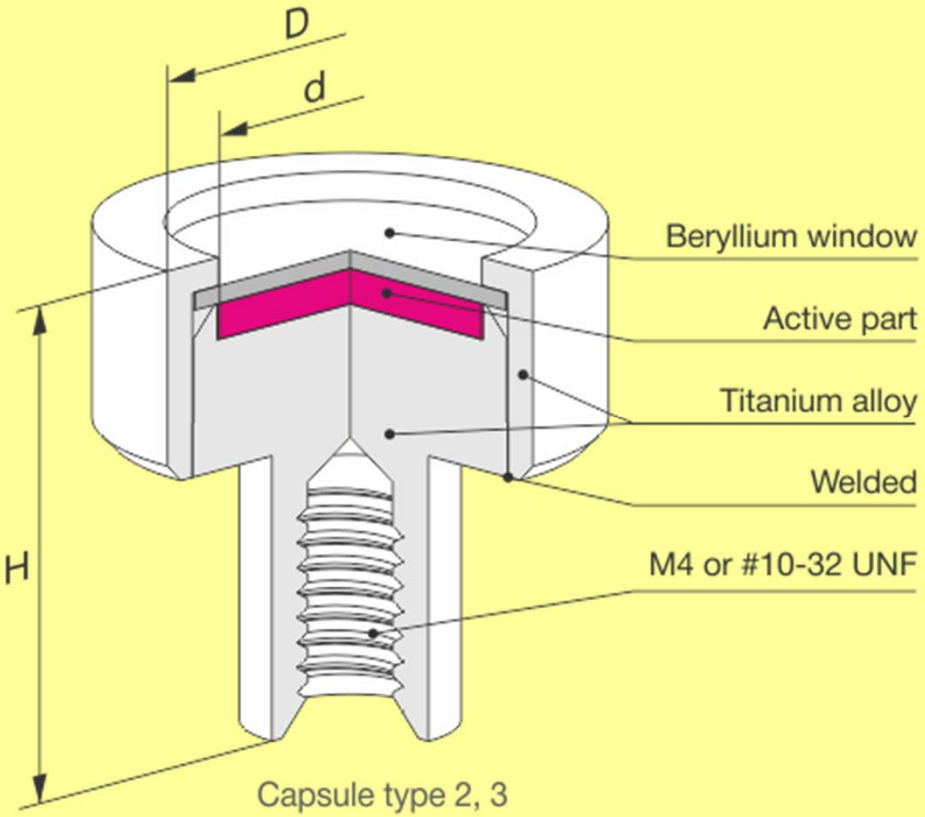

Mean Lifetime τ of Excited State and Natural Line Width Γ

An excited state (nuclear or electronic) of mean lifetime τ does not have a sharp energy value, but only a value within the energy range ΔE

the **Heisenberg Uncertainty Principle:**
$\Delta \mathbf{E} \, \Delta \mathbf{t} \geq \hbar$

natural line width $\Gamma = \hbar / \tau$

Transitions from an excited (e) to the ground state (g) involve all energies within the range of ΔE

The transition probability or intensity as a function of E = a spectral line centered around the most probable transition energy E_0

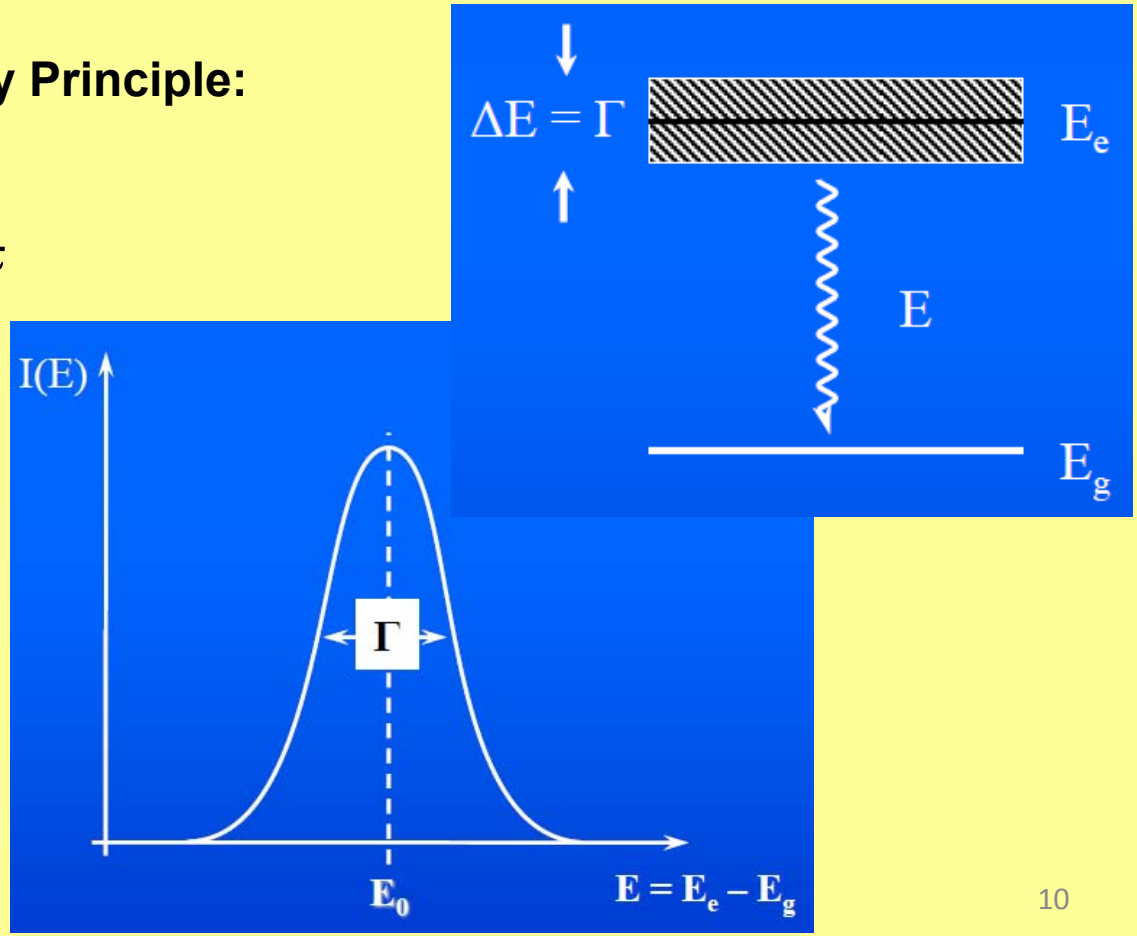

Transition Probability

Lorentzian formula for spectral line shape

$$I(E) = \frac{(\Gamma/2)^2}{(E - E_0)^2 + (\Gamma/2)^2}$$

The width at half maximum of the spectral line = natural line width Γ determined by the mean lifetime τ

^{57}Fe (14.4 keV)

τ =1.43 10^{-7} s

Γ = 4.6 10^{-9} eV

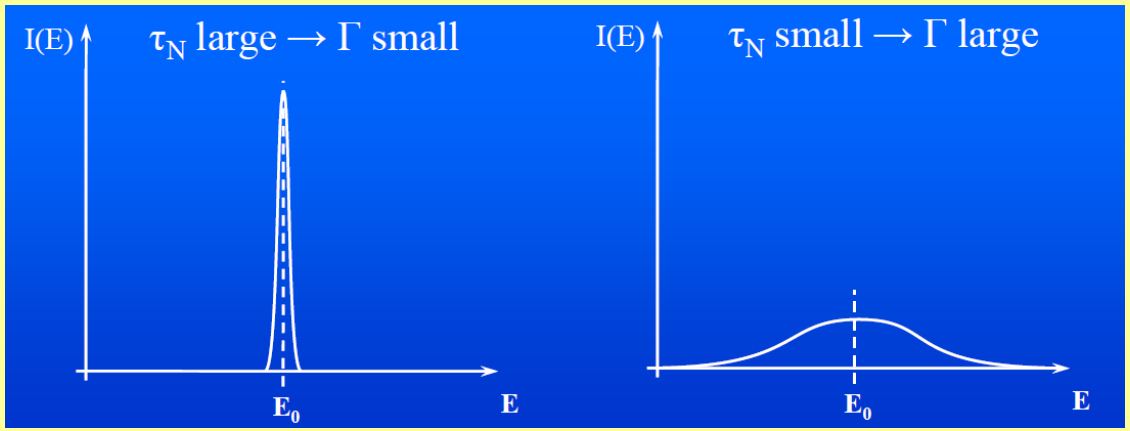

Resonance absorption is observable only if the emission and absorption lines **overlap sufficiently**. This is not the case when the lines are too narrow or too broad

Suitable for Mössbauer spectroscopy: lifetime = 10^{-6} - 10^{-11} s

Recoil Effect

^{57}Fe (14.4 keV)
Γ = 4.6 10^{-9} eV

$$E_R = \frac{E_\gamma^2}{2mc^2}$$

Recoil energy E_R = 2 10^{-3} eV
Much larger (5-6 orders of magnitude) than the natural line width
= no resonance possible between free atoms

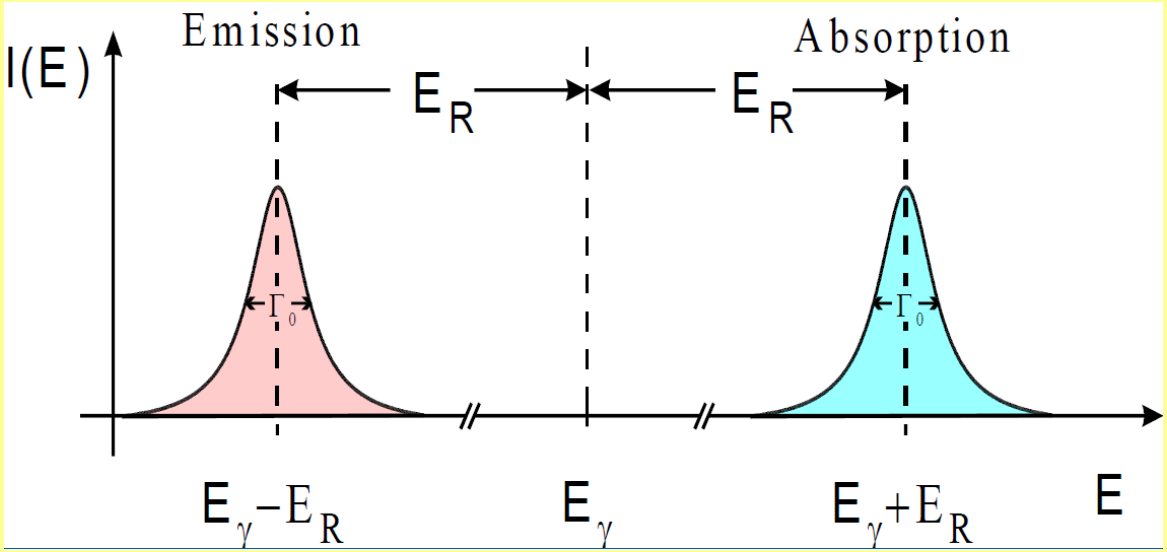

The Mössbauer effect cannot be observed for freely moving atoms or molecules, i.e. in gaseous or liquid state

Recoil Effect

^{57}Fe (14.4 keV)
Γ = 4.6 10^{-9} eV

$$E_R = \frac{E_\gamma^2}{2mc^2}$$

Recoil energy $E_R = 2 \times 10^{-3}$ eV
Much larger (5-6 orders of magnitude) than the natural line width
= no resonance possible between free atoms

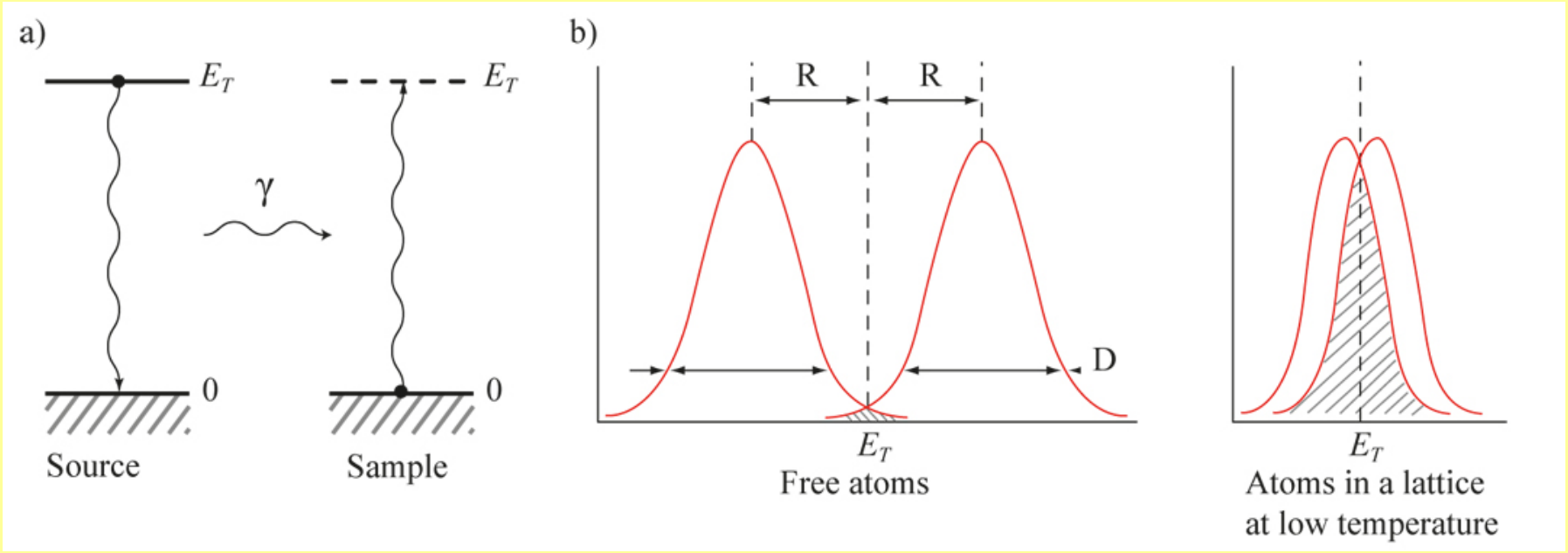

The Mössbauer effect cannot be observed for freely moving atoms or molecules, i.e. in gaseous or liquid state

Recoilless Emission and Absorption

Solid state, crystalline or non-crystalline = atoms tightly bound in the lattice
Unshifted transition lines overlap = nuclear resonance absorption observed

$$E_R = \frac{E_\gamma^2}{2mc^2}$$

Large mass M of a solid particle as compared to an atom = the linear momentum created by emission and absorption of a gamma quantum practically vanishes

The recoil energy is mostly transferred to the lattice vibrational system.
The vibrational energy of the lattice can only change by discrete amounts 0, $\pm\hbar\omega$, $\pm 2\hbar\omega$, …

The probability *f* (Debye-Waller or Lamb-Mössbauer factor) that no lattice excitation (zero-phonon processes) takes place during γ-emission or absorption.

f denotes the fraction of nuclear transitions which occur without recoil. Only for this fraction is the Mössbauer effect observable.

Debye-Waller or Lamb-Mössbauer Factor

$$f = \exp\left[-\frac{E_R}{k_B \Theta_D}\left(\frac{3}{2}+\frac{\pi^2 T^2}{\Theta_D^2}\right)\right]$$

f increases with:

* decreasing recoil energy E_R
* decreasing temperature T
* increasing Debye temperature $\theta_D = h\omega_D/2\pi k_B$

ω_D = vibrational frequency of Debye oscillator, k_B = Boltzmann factor

θ_D = a measure for the strength of the bonds between the Mössbauer atom and the lattice

Mössbauer-Experiment

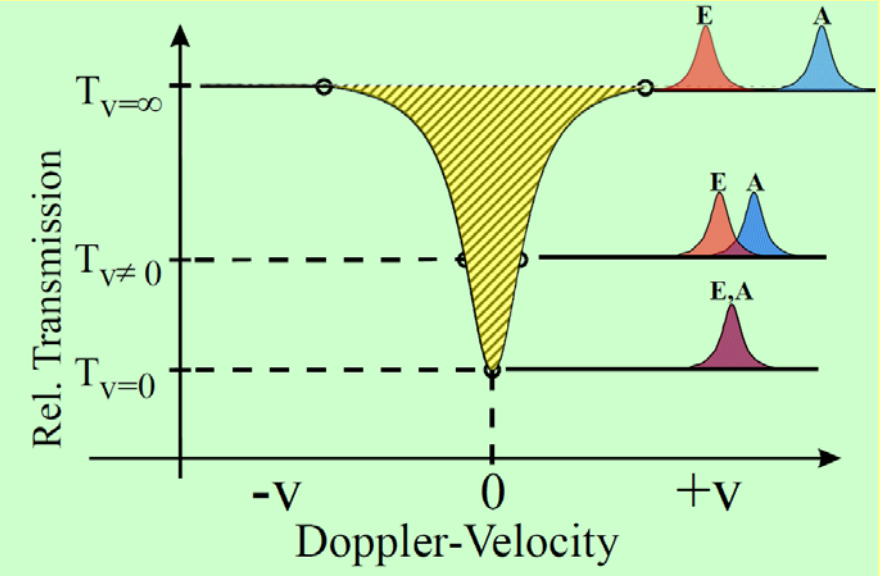

The resonance perturbed by electric and magnetic **hyperfine interactions** between the nuclei and electric and magnetic fields set up by electrons

Hyperfine interactions **shift** and **split** degenerate nuclear levels resulting in several transition lines

The Mössbauer source emits a single transition line E (assume the absorber shows also only one transition line A).

E and A have slightly modified transition energies, perturbation energies 10^{-8} eV comparable to the natural linewidth, shifts the transition lines away from each other such that the overlap decreases or disappears entirely

Overlap restored by the **Doppler effect**, i.e. by moving the absorber and the source relative to each other

Mössbauer-Experiment

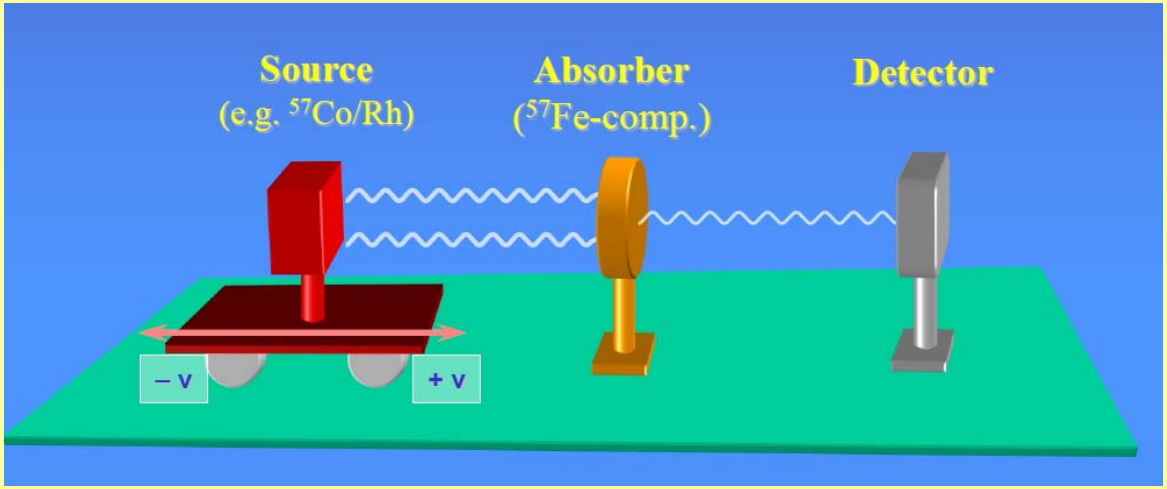

Source and absorber are moved relative to each other

Doppler velocity

$$v = c\frac{\Gamma_0}{E_\gamma}$$

^{57}Fe : $\Gamma_0 = 4.7 \cdot 10^{-9}$ eV, $E_\gamma = 14400$ eV, ***v* = 0.096 mm s^{-1}**
c = speed of light

Mössbauer-Experiment

4.2 K b.p. of liquid He
1.5 K by pumping on the liquid He vessel

controls the electro-mechanical vibrator

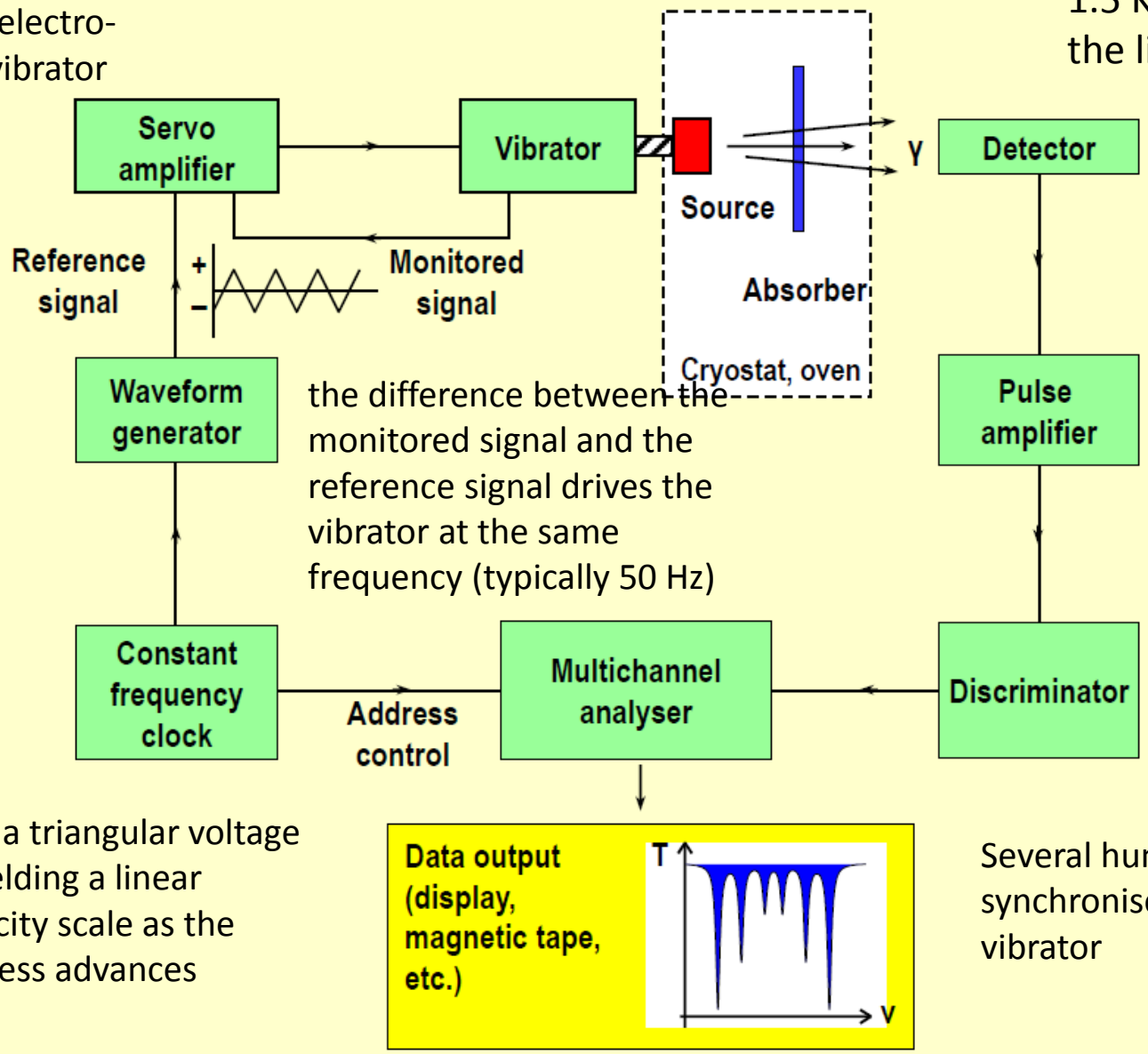

the difference between the monitored signal and the reference signal drives the vibrator at the same frequency (typically 50 Hz)

Non-resonant background radiation rejected

synchronises a triangular voltage waveform yielding a linear Doppler velocity scale as the channel address advances

Several hundred channels synchronised with the vibrator

Mössbauer-Experiment

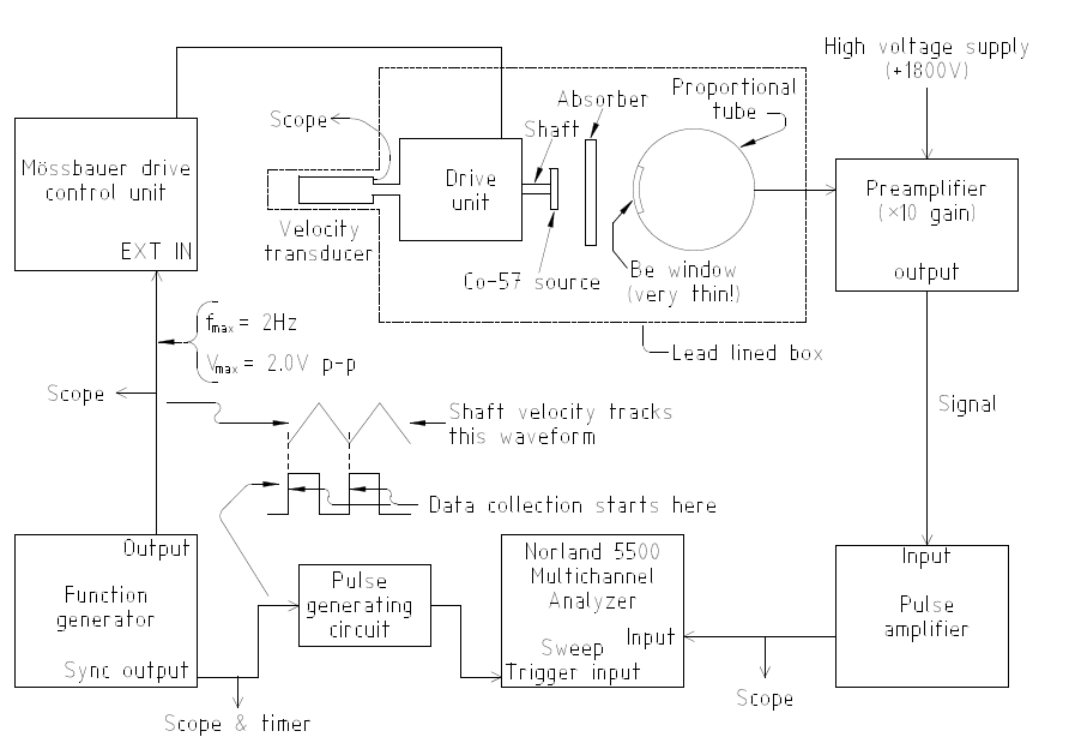

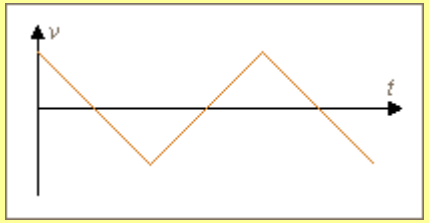

Constant acceleration

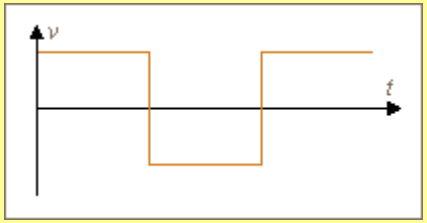

Constant velocity

Mössbauer-Experiment

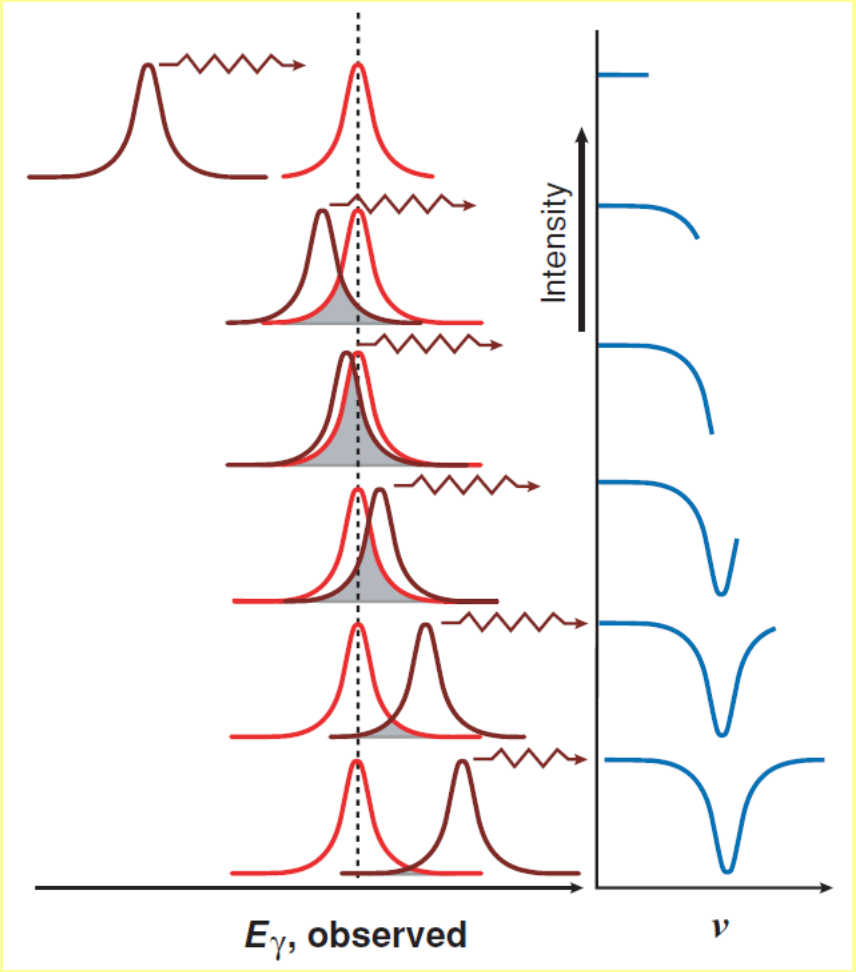

the source is moved to Doppler shift the center of the emission spectrum (*brown*) from smaller to larger energies, relative to the center of the absorption spectrum (*red*), whose center, the quantized transition energy, is fixed. The level of the transmission spectrum (*blue*) at each value of velocity, *v*, is determined by how much the shifted emission spectrum overlaps the absorption spectrum, such that greater overlap results in reduced transmission owing to resonant absorption. The evolution of the transmission spectrum from large negative (source moving away from absorber) to large positive values of velocity may be followed from the top to the bottom rows.

Correlation of count rate with channel number and relative velocity

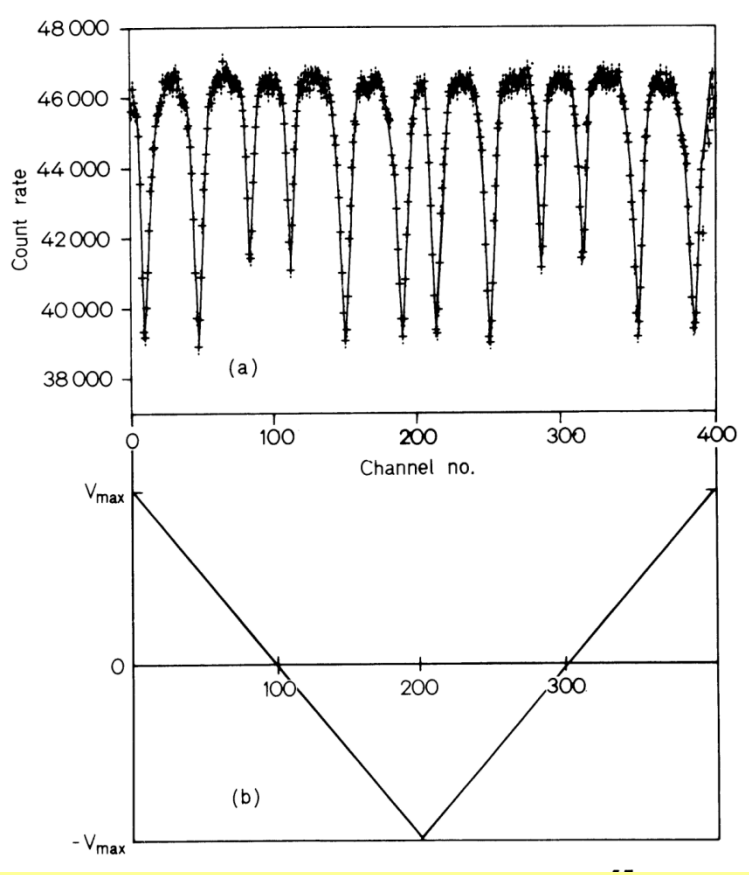

Mössbauer spectrum of metallic Fe. The count rate is plotted as function of the channel number

Doppler velocity as a function of the channel number

Hyperfine Interactions between Nuclei and Electrons

Mössbauer Parameters

—Electric Monopole Interaction = Isomer Shift δ

—Electric Quadrupole Interaction = Quadrupole Splitting ΔE_Q

—Magnetic Dipole Interaction = Magnetic Splitting ΔE_M

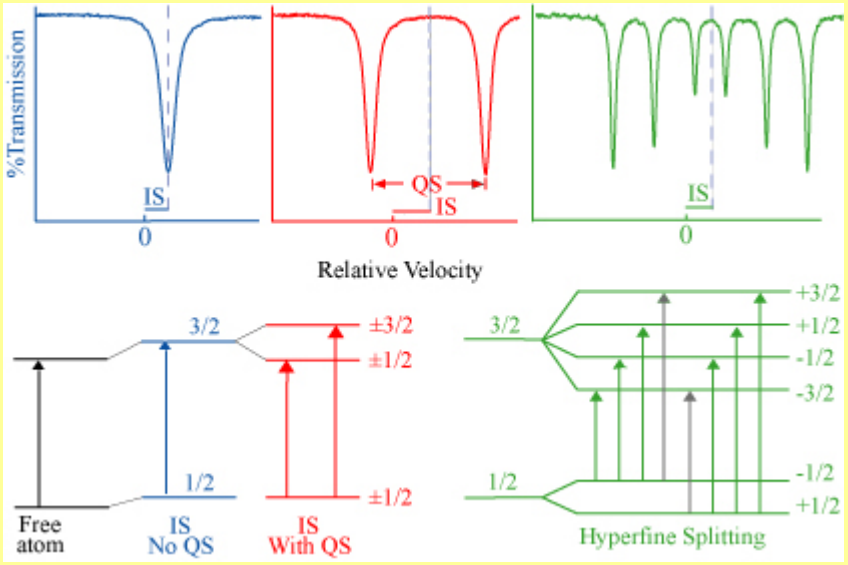

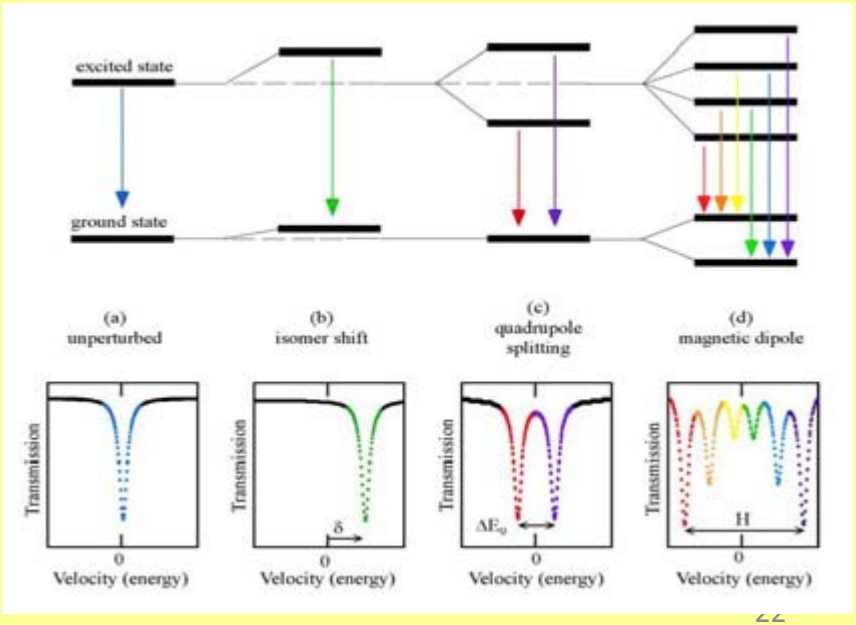

Hyperfine Interactions

Electric monopole interaction (Coulombic)
between protons of the nucleus and s-electrons penetrating the nuclear field.
Different shifts of nuclear levels A and E.
Isomer shift values give information on the oxidation state, spin state, and bonding properties, such as covalency and electronegativity.

Electric quadrupole interaction
between the nuclear quadrupole moment ($eQ \neq 0$, $I > ½$) and an inhomogeneous electric field at the nucleus ($EFG \neq 0$). Nuclear states split into $I + ½$ substates.
The quadrupole splitting gives the information on oxidation state, spin state and site symmetry.

Magnetic dipole interaction
between the nuclear magnetic dipole moment ($\mu \neq 0$, $I > 0$) and a magnetic field ($H \neq 0$) at the nucleus. Nuclear states split into $2I+1$ substates with $m_I = +I, +I-1, \ldots, -I$
The magnetic splitting gives information on the magnetic properties of the material under study - ferromagnetism, antiferromagnetism.

Isomer Shift

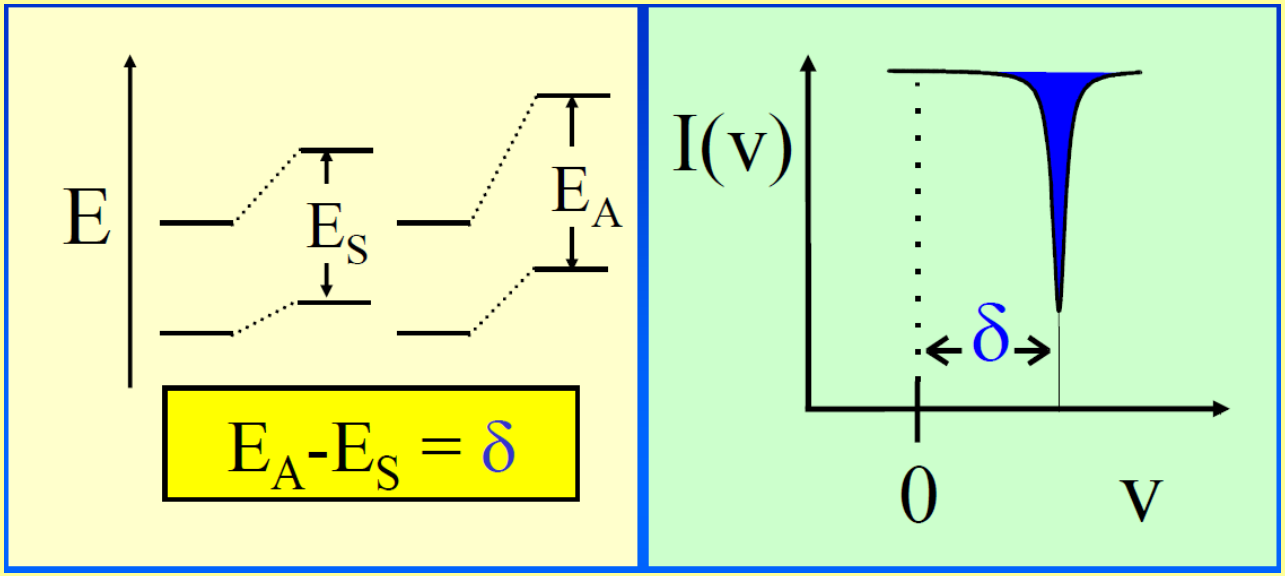

The nuclear radius in the excited state is different (in ^{57}Fe smaller) than that in the ground state: $R_e \neq R_g$.
The electronic densities of all s-electrons (1s, 2s, 3s, etc.) are different at the nuclei of the source and the absorber: $\rho_S \neq \rho_A$.
The result is that the electric monopole interactions (Coulomb interactions) are different in the source and the absorber and therefore affect the nuclear ground and excited state levels to a different extent. This leads to the measured isomer shift δ.

Isomer Shift

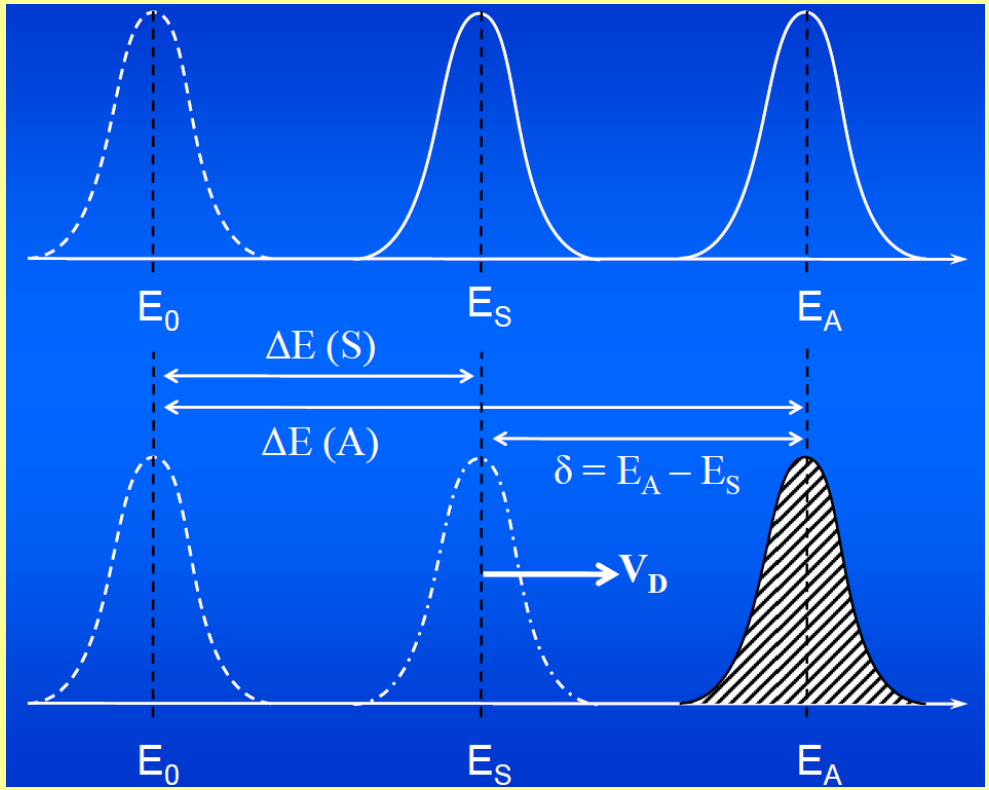

$\delta = E_A - E_S = C\,(\rho_A - \rho_S)(R_e^2 - R_g^2)$

$C = (2/3)\pi Z e^2$.

The energy levels of the ground and excited states of a bare nucleus are perturbed and shifted by electric monopole interactions. The shifts in the ground and excited states differ = different nuclear radii and different Coulombic interactions.

The energy differences E_S and E_A in the source and absorber also differ because of the different electron densities in the source and absorber material.

The individual energy differences E_S and E_A cannot be measured individually, a Mössbauer experiment measures only the difference of the transition energies $\delta = E_A - E_S$, isomer shift.

Isomer Shift

The isomer shift depends directly on the s-electron densities and are influenced indirectly via shielding by p-, d-, and f-electrons which are not capable (relativistic effects) of penetrating the nuclear field.

$$\delta = C\,\{|\Psi(0)|_A^2 - |\Psi(0)|_S^2\}(R_e^2 - R_g^2)$$

Influence on $|\Psi(0)|^2$:

Direct = change of electron population in *s*-orbitals (mainly valence *s*-orbitals) changes directly $|\Psi(0)|^2$

Indirect = shielding by *p-, d-, f*-electrons, increase of electron density in *p-, d-, f*-orbitals increases shielding effect for *s*-electrons from the nuclear charge
→ *s*-electron cloud expands, $|\boldsymbol{\Psi(0)|^2}$ at nucleus decreases.

^{119}Sn Mössbauer Spectra

$(R_e^2 - R_g^2) > 0$

$$\delta = C\{|\Psi(0)|_A^2 - |\Psi(0)|_S^2\}(R_e^2 - R_g^2)$$

Compound	δ/ mm s^{-1}		Compound	δ/ mm s^{-1}
SnF_4	–0.36		Sn (metal)	2.50
SnO_2	0.0		Sn (gray)	2.02
$SnCl_4$	0.85		SnO	2.71
$SnBr_4$	1.15		$SnSO_4$	3.90
SnI_4	1.55		SnF_2	3.2
$SnPh_4$	1.22		$SnCl_2$	4.07
SnH_4	1.27		$SnBr_2$	3.93

Sn(IV) $\delta <$ 2.00 mm s^{-1} electron config. 5s^0 – lower el. density at nucleus than neutral atom = negative shift

Sn(II) $\delta >$ 2.50 mm s^{-1} electron config. 5s^2 – higher el. density at nucleus than neutral atom as no 5p shielding = positive shift

^{119}Sn Mössbauer Spectra

$(R_e^2 - R_g^2) > 0$

$$\delta = C\{|\Psi(0)|_A^2 - |\Psi(0)|_S^2\}(R_e^2 - R_g^2)$$

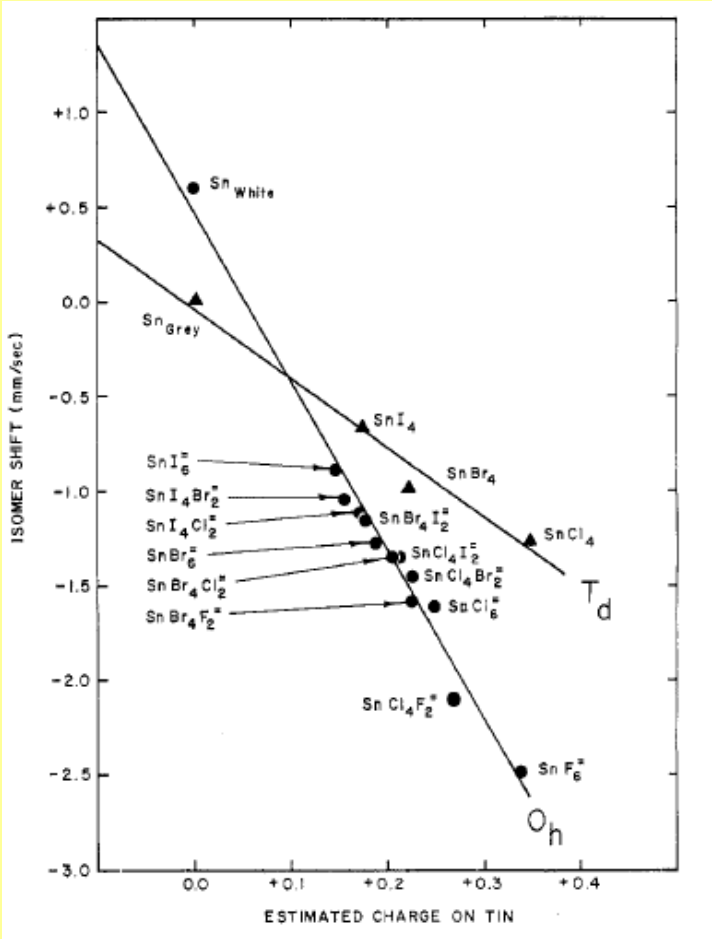

^{119}Sn Mössbauer Spectra

$(R_e^2 - R_g^2) > 0$

$$\delta = C\{|\Psi(0)|_A^2 - |\Psi(0)|_S^2\}(R_e^2 - R_g^2)$$

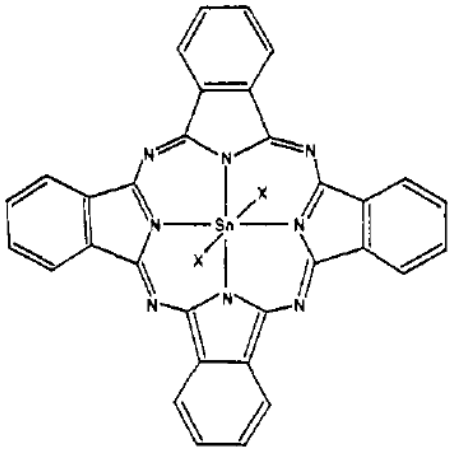

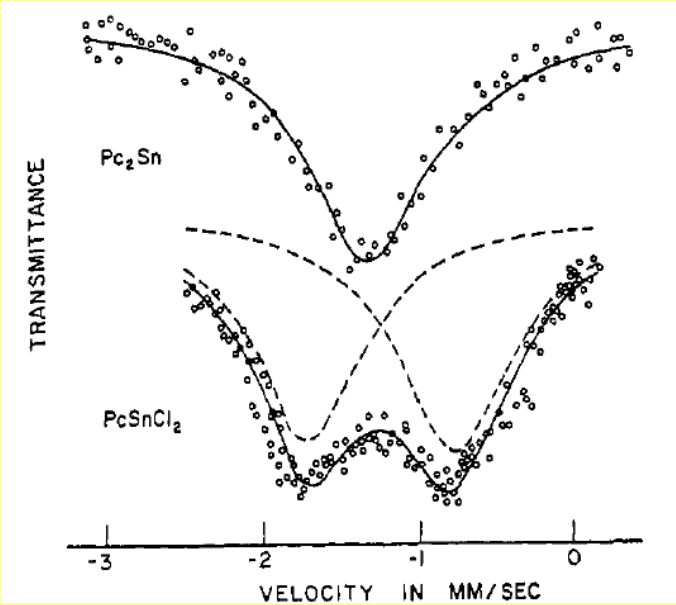

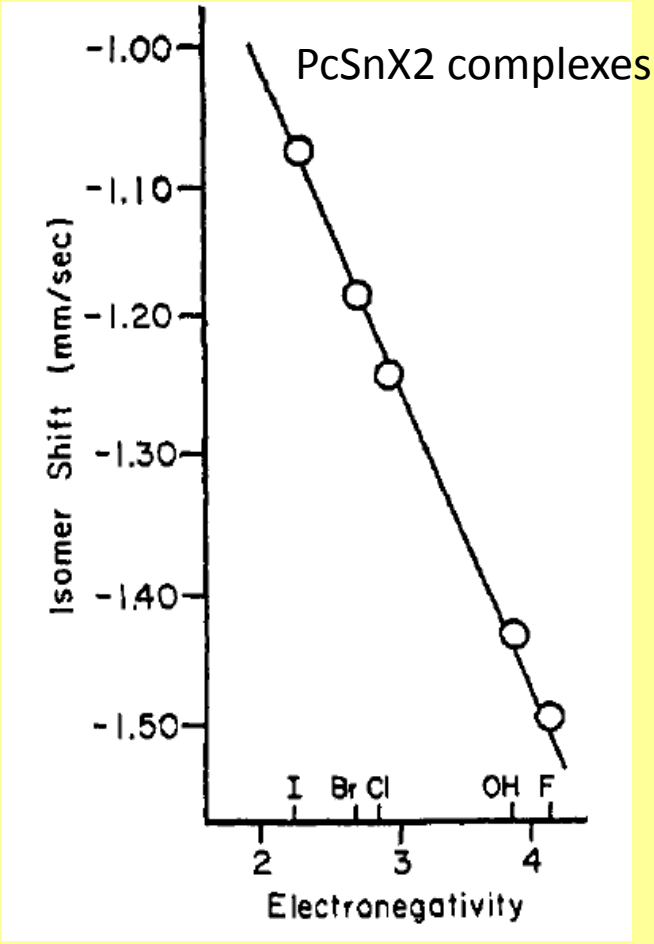

^{119}Sn Mössbauer Spectra

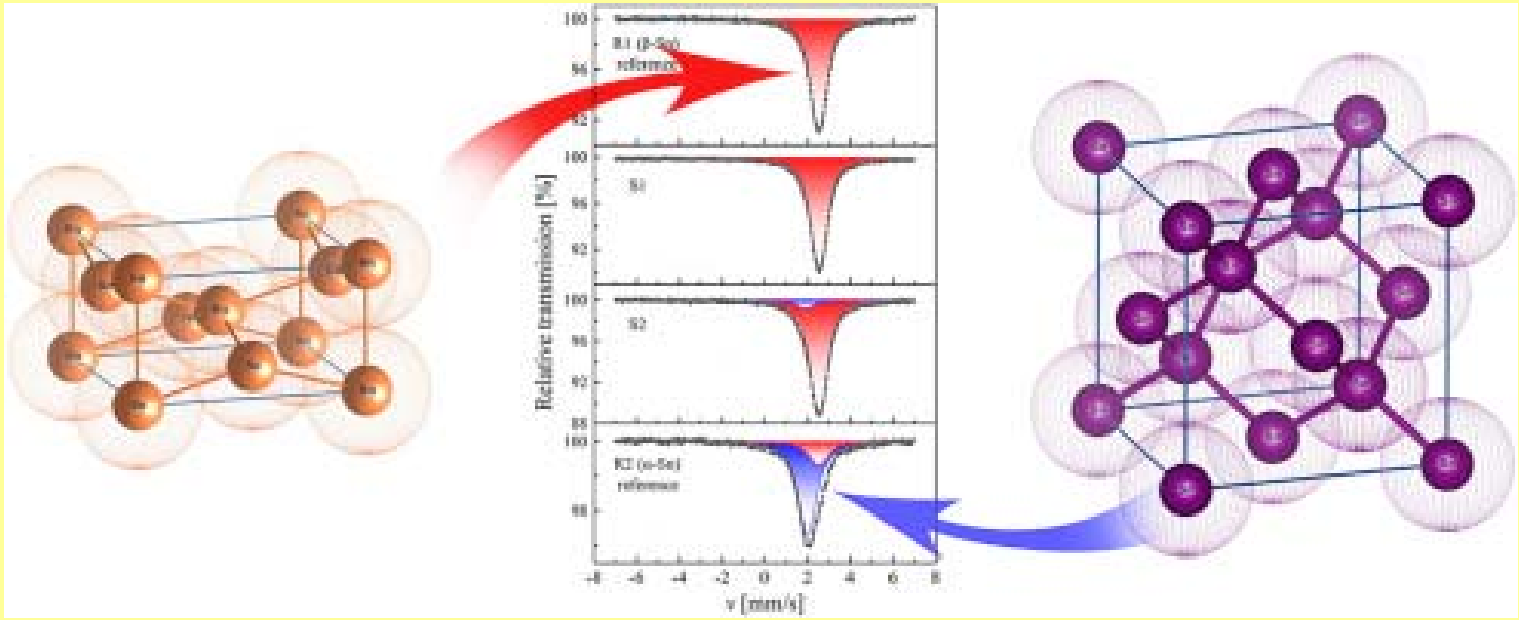

10.1016/j.matchemphys.2016.07.061

JACS 1970,92,1501
IC1971,10,1553

Electron Densities at the Nucleus (r = 0)

Electrons per cubic Bohr radius	$3d^8$	$3d^7$ Fe^+	$3d^6$ Fe^{2+}	$3d^5$ Fe^{3+}	$3d^6 4s^2$ free atom
$\lvert\psi_{1s}(0)\rvert^2$	5378.005	5377.973	5377.840	5377.625	5377.873
$\lvert\psi_{2s}(0)\rvert^2$	493.953	493.873	493.796	493.793	493.968
$\lvert\psi_{3s}(0)\rvert^2$	67.524	67.764	68.274	69.433	68.028
$\lvert\psi_{4s}(0)\rvert^2$					3.042
$2\sum_n \lvert\psi_{ns}(0)\rvert^2$	11878.9	11879.2	11879.8	11881.7	11885.8

[1] Watson, R. E. (1960) *Phys. Rev.*, **118**, 1036.
[2] Watson, R. E. (1960) *Phys. Rev.*, **119**, 1934.

The partial electron densities refer to one electron each in 1s, 2s, 3s, 4s-orbitals. The total s-electron density at r = 0 is twice the sum of the partial one-electron contributions (all s-orbitals are doubly occupied).

Isomer Shifts of Iron Compounds

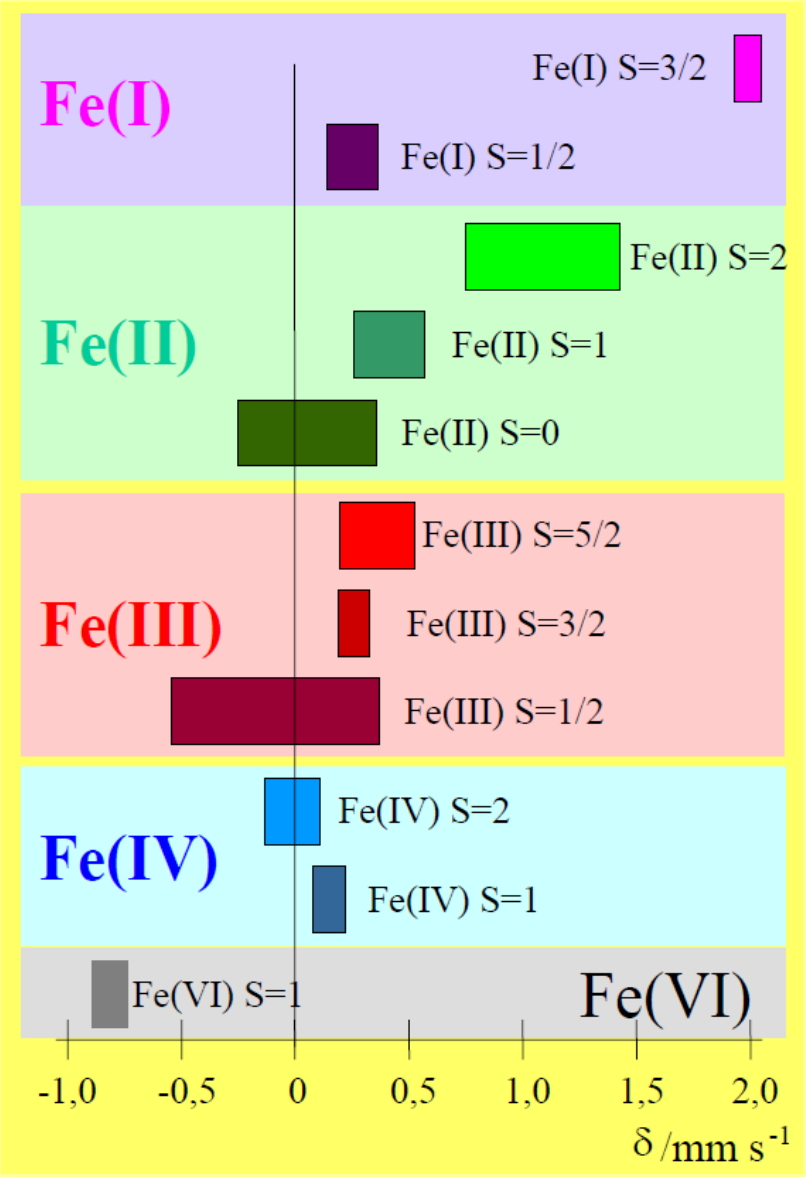

The most positive isomer shift occurs with iron(I) with spin S = 3/2.
The seven d-electrons exert a very strong shielding of the s-electrons, this reduces the s-electron density ρ_A giving a strongly negative quantity $(\rho_A - \rho_S)$, as $(R_e^2 - R_g^2) < 0$ for ^{57}Fe, the isomer shift becomes strongly positive.

Strongly negative for iron(VI) with spin S = 1.
There are only two d-electrons, the shielding effect for s-electrons is very weak and the s-electron density ρA at the nucleus becomes high.

Iron(II) high spin with S=2 can be easily assigned.
In other cases with overlapping δ values ambiguous assignment. Need to consider the quadrupole splitting parameter.

Effect of Ligand Electronegativity

$$\delta = C\,\{|\Psi(0)|_A^2 - |\Psi(0)|_S^2\}(R_e^2 - R_g^2)$$

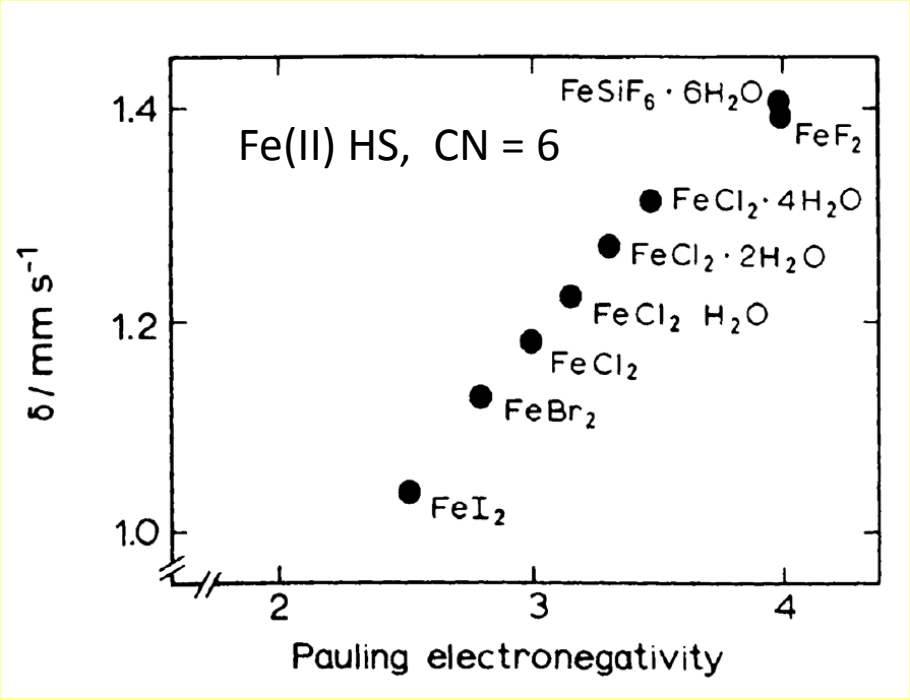

The electronegativity increases from I to F

In the same ordering the 4s-electron population decreases and the s-electron density at the iron nucleus decreases

$(R_e^2 - R_g^2) < 0$ for ^{57}Fe

the isomer shift increases from iodide to fluoride.

Second-Order Doppler Shift

The isomer shifts δ, i.e. the resonance peak shifts observed in Mössbauer spectra, are composed of two terms:

$\delta = \delta_C + \delta_{SOD}(T)$

The first term is the ***chemical isomer shift*** $\boldsymbol{\delta_C}$ which is temperature-independent.
The second term is the ***second-order Doppler shift*** $\boldsymbol{\delta_{SOD}}$.
Since δ_{SOD} is T-dependent, the observed isomer shift δ is also T-dependent.

The **second-order Doppler shift** δ_{SOD} is related to the mean-square velocity $\langle \boldsymbol{v^2} \rangle$ of lattice vibrations in the direction of the γ-ray propagation which increases with increasing T. Accordingly, the Mössbauer resonance moves to a more negative velocity with increasing T :

$$\delta_{SOD} = -\frac{\langle v^2 \rangle}{2c}$$

Electric Quadrupole Interaction

Quadrupole Splitting ΔE_Q

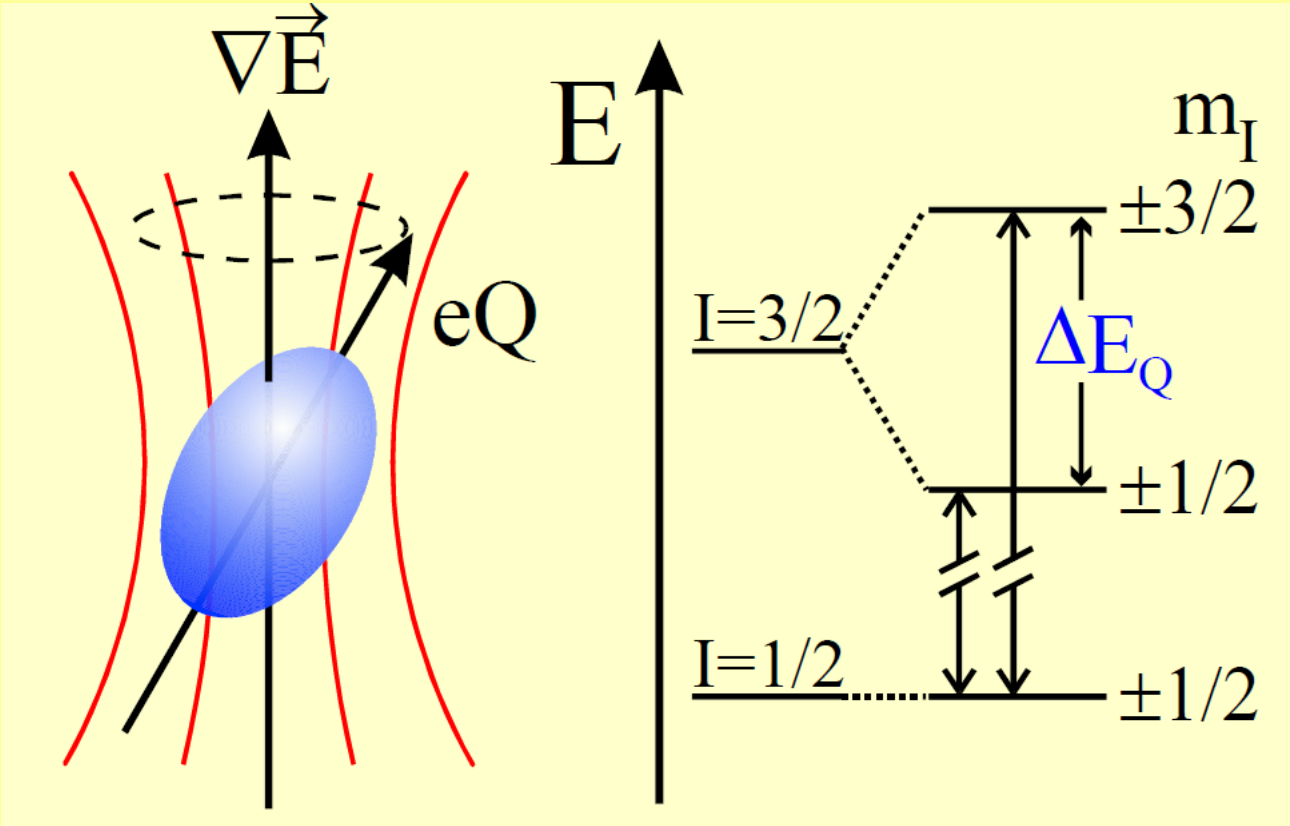

Electric Quadrupole Interaction

Electric quadrupole interaction occurs if at least one of the nuclear states involved possesses a quadrupole moment eQ (for I > 1/2) and if the electric field at the nucleus is inhomogeneous.

^{57}Fe: the first excited state (14.4 keV) has a spin I = 3/2 and therefore also an electric quadrupole moment eQ.

Quadrupole Splitting ΔE_Q
EFG is non-zero in non-cubic valence electron distribution and/or in non-cubic lattice site symmetry

The precession of the quadrupole moment vector about the field gradient axis

Splits the degenerate I = 3/2 level into two substates with magnetic spin quantum numbers $m_I = \pm 3/2$ and $\pm 1/2$.

Selection rule: $\Delta m_I = 0, \pm 1$

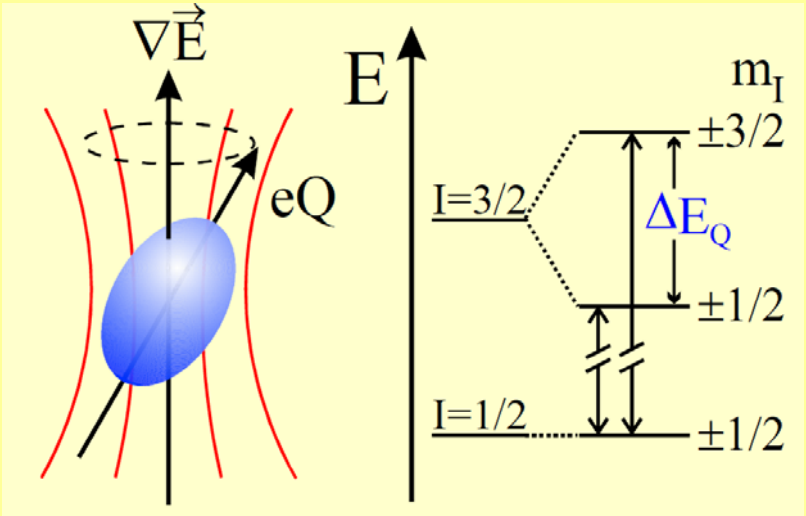

The ground state I = ½
-no quadrupole moment
-unsplit
-twofold degenerate

Electric Quadrupole Interaction

Quadrupole Splitting ΔEQ

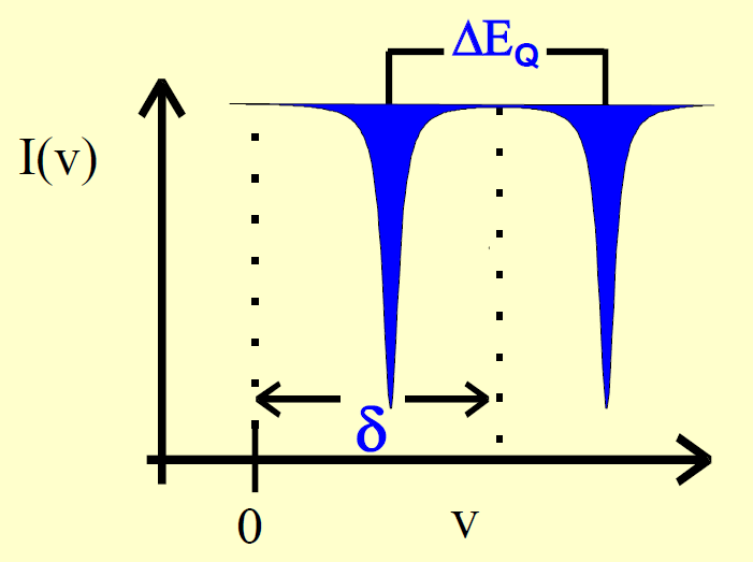

The energy difference between the two substates ΔE_Q is observed in the spectrum as the separation between the two resonance lines

$$E_Q(I, m_I) = \frac{eQV_{zz}}{4I(2I-1)}\left[3m_I^2 - I(I+1)\left(1+\frac{\eta^2}{3}\right)^{\frac{1}{2}}\right.$$

Electric Field Gradient (EFG)

A point charge q at a distance $r = (x^2 + y^2 + z^2)^{1/2}$ from the nucleus causes a potencial V(r) = q/r at the nucleus. The electric field E at the nucleus is the negative gradient of the potential, $-\nabla V$, and the electric field gradient EFG is given by:

$$EFG = \vec{\nabla}\vec{E} = -\vec{\nabla}\vec{\nabla}V = \begin{vmatrix} V_{xx} & V_{xy} & V_{xz} \\ V_{yx} & V_{yy} & V_{yz} \\ V_{zx} & V_{zy} & V_{zz} \end{vmatrix}$$

$V_{ij} = (\partial^2 V/\partial_i \partial_j)$ (i,j,k = x,y,z)
3x3 second rank EFG tensor

Only five V_{ij} components are independent, because:
- symmetric form of the tensor, i.e. $V_{ij} = V_{ji}$,
- Laplace: traceless tensor

$$\sum_i V_{ii} = 0, \quad i = x, y, z$$

Principal axes system: $|V_{zz}| \geq |V_{xx}| \geq |V_{yy}|$
Axial symmetry (tetragonal, trigonal) - the EFG is given only by the tensor component V_{zz} , $V_{xx} = V_{yy} \rightarrow \eta = 0$

Non-axial symmetry – the asymmetry parameter η: $0 \leq \eta \leq 1$
$\eta = (V_{xx} - V_{yy})/V_{zz}$

Electric Field Gradient (EFG)

Two kinds of contributions to the EFG: $\mathbf{(EFG)_{total} = (EFG)_{val} + (EFG)_{lat}}$

or in the principal axes system and η = 0: $\mathbf{(Vzz)_{total} = (Vzz)_{val} + (Vzz)_{lat}}$

The **lattice contribution** $\mathbf{(V_{zz})_{lat}}$ = non-cubic arrangement of the next nearest neighbours

The **valence contribution** $\mathbf{(V_{zz})_{val}}$ = anisotropic (noncubic) electron population in the orbitals

Energy levels

$$E_Q(I, m_I) = \frac{eQV_{zz}}{4I(2I-1)}\left[3m_I^2 - I(I+1)\left(1+\frac{\eta^2}{3}\right)^{\frac{1}{2}}\right]$$

Electric Field Gradient (EFG)

For ^{57}Fe with $I_e = 3/2$, $I_g = 1/2$:

$E_Q\,(3/2, \pm 3/2) = 3eQV_{zz}/12$ for $I = 3/2$, $m_I = \pm 3/2$

$E_Q\,(3/2, \pm 1/2) = -3eQV_{zz}/12$ for $I = 3/2$, $m_I = \pm 1/2$

the **quadrupole splitting energy**

$\Delta E_Q = E_Q(3/2, \pm 3/2) - E_Q\,(3/2, \pm 1/2) = eQV_{zz}/2$

(in axially symmetric systems, $\eta = 0$)

$$E_Q(I, m_I) = \frac{eQV_{zz}}{4I(2I-1)}\left[3m_I^2 - I(I+1)\right]\left(1+\frac{\eta^2}{3}\right)^{\frac{1}{2}}$$

$[Fe(H_2O)_6]^{3+}$ $^6A_1$

$[ML_6]$ (O_h)

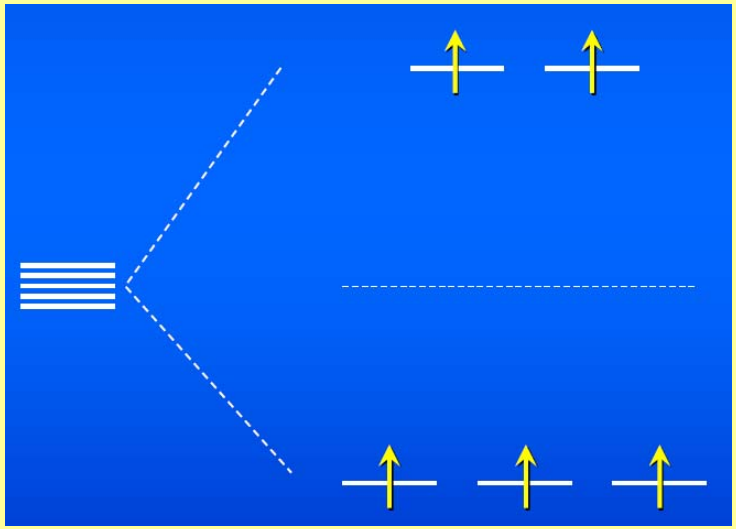

z2
x2–y2

xz
yz
xy

$EFG_{lat} = 0$

$EFG_{val} = 0$

$FeSO_4 \cdot 7H_2O$

$[Fe(H_2O)_6]^{2+}$ Fe(II)-HS, S = 2

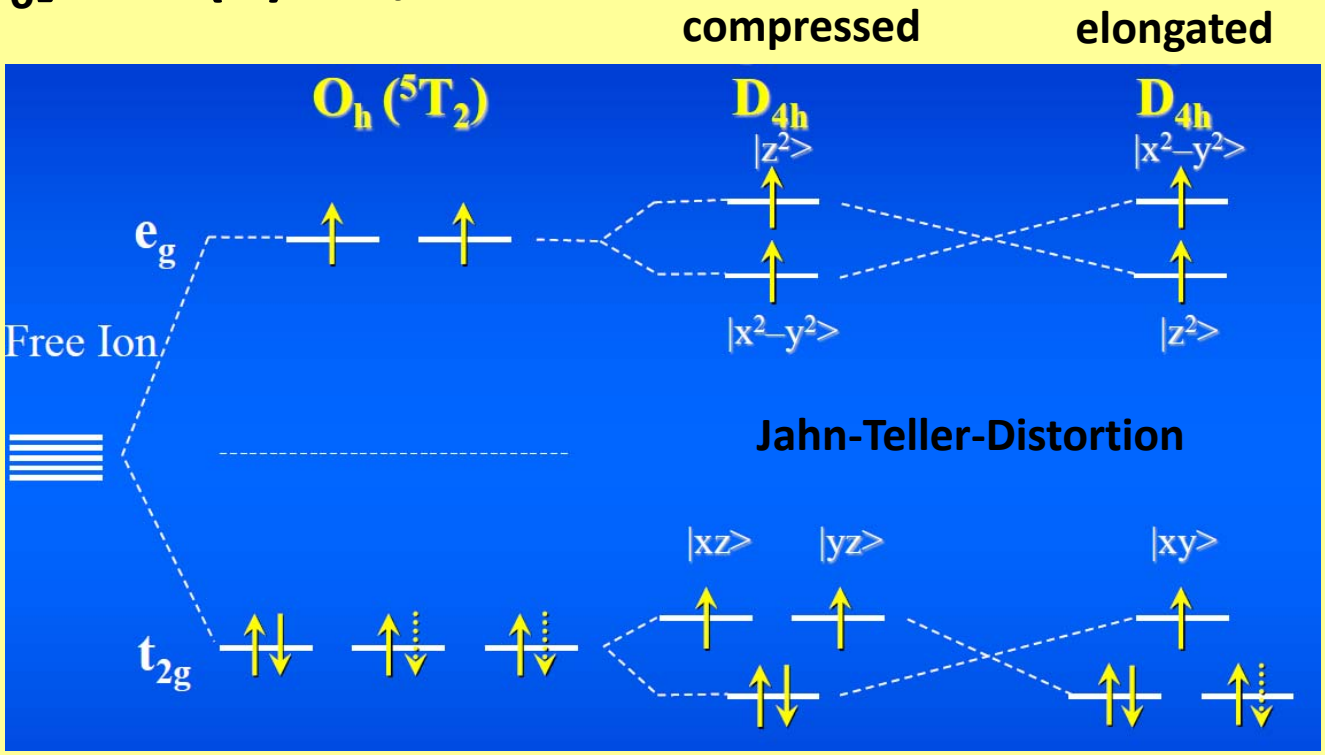

EFG_{lat}	$= 0$	$\neq 0$
EFG_{val}	$\neq 0$	$\neq 0$

$FeSO_4 \cdot 7H_2O$

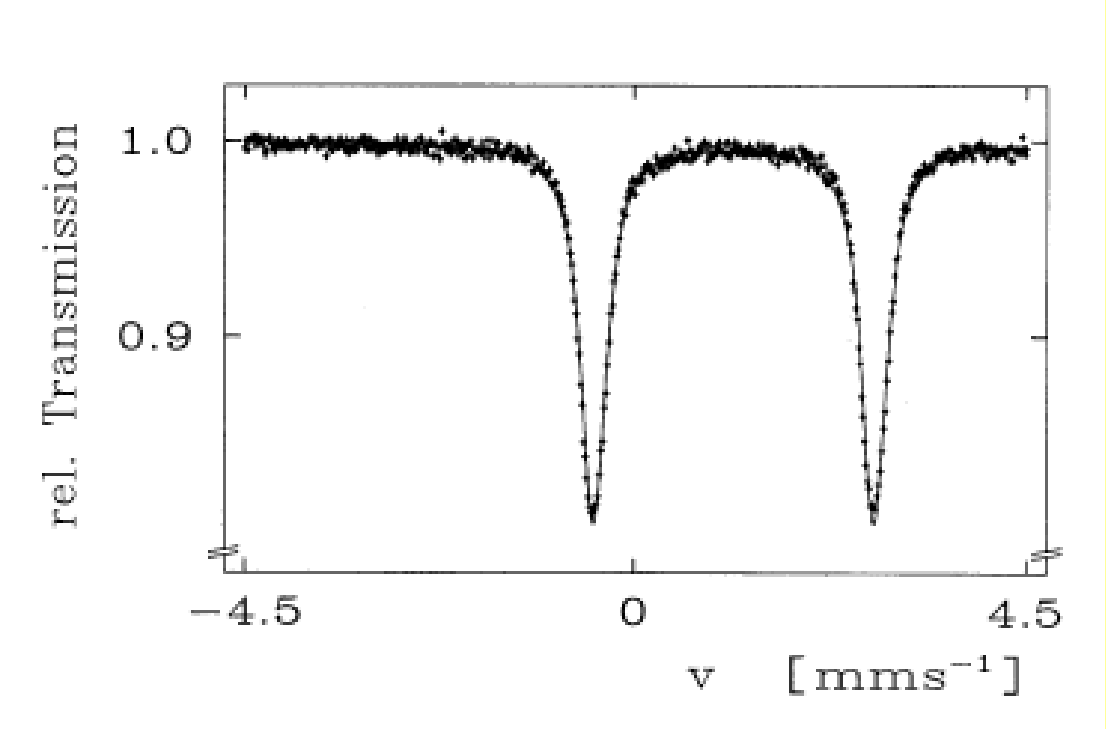

$K_4[Fe(CN)_6]$

Fe(II)-LS, S = 0 cubic

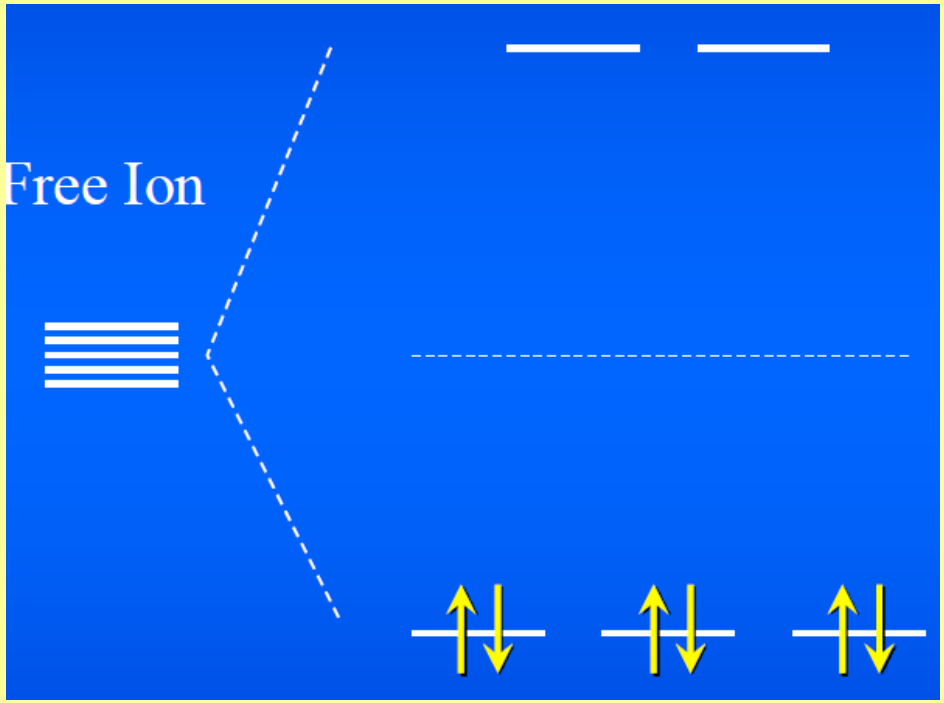

EFG_{lat} = 0

EFG_{val} = 0

$K_4[Fe(CN)_6]$

Fe(II)-LS, S = 0 cubic

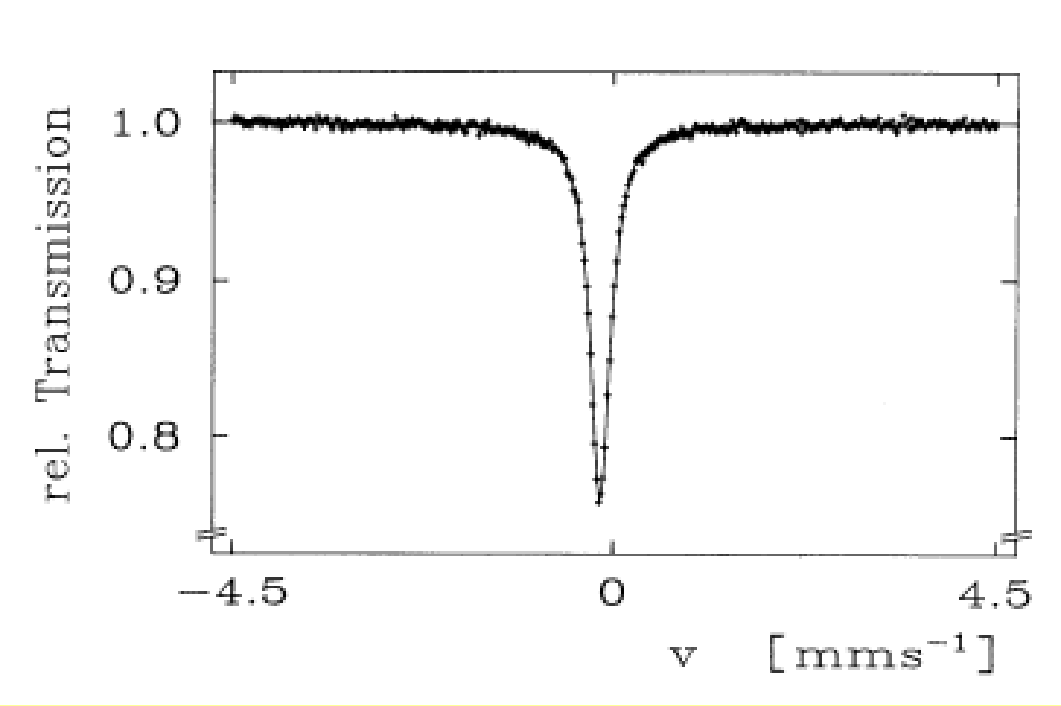

$Na_2[Fe(CN)_5(NO)]$

Fe(II)-LS, S = 0 tetragonal

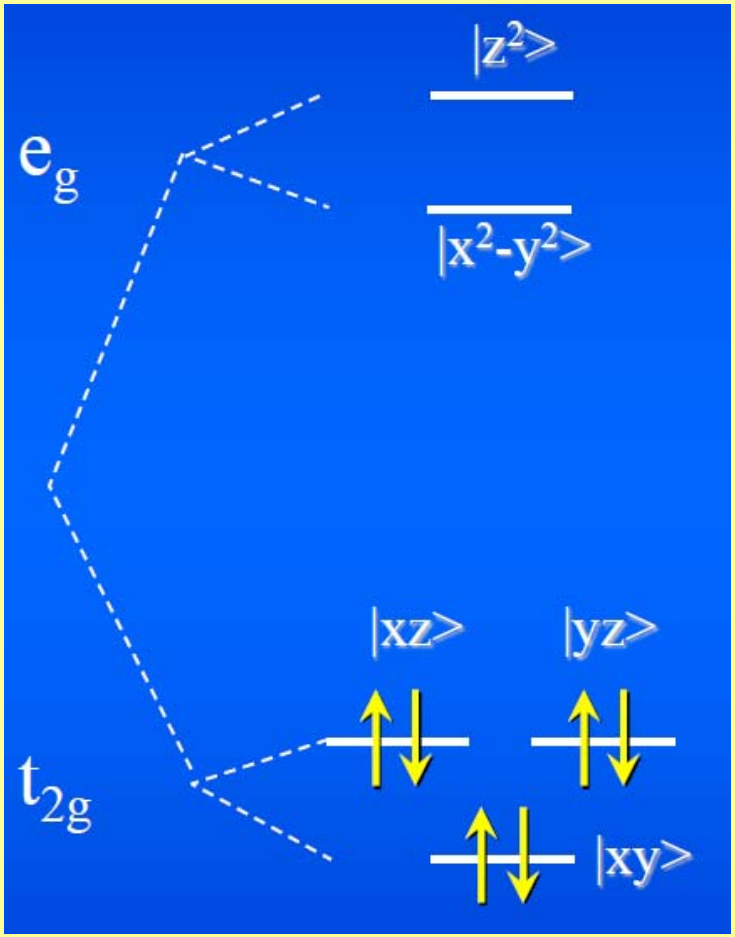

Fe(II) + NO^+

or

Fe(III) + NO

$EFG_{lat} \neq 0$

$EFG_{val} \neq 0$

$Na_2[Fe(CN)_5(NO)]$

Fe(II)-LS, S = 0 tetragonal

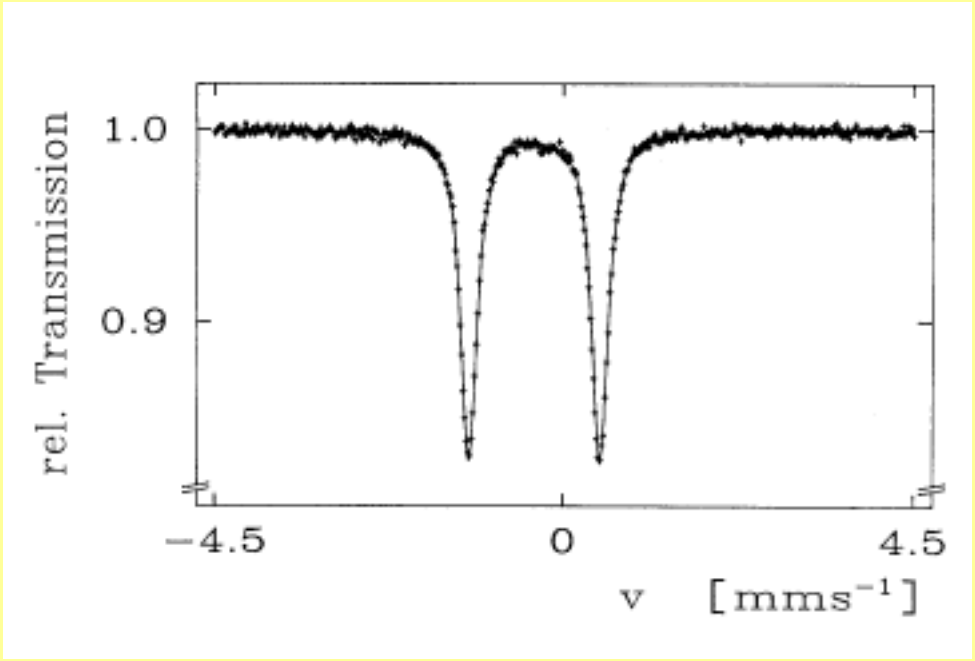

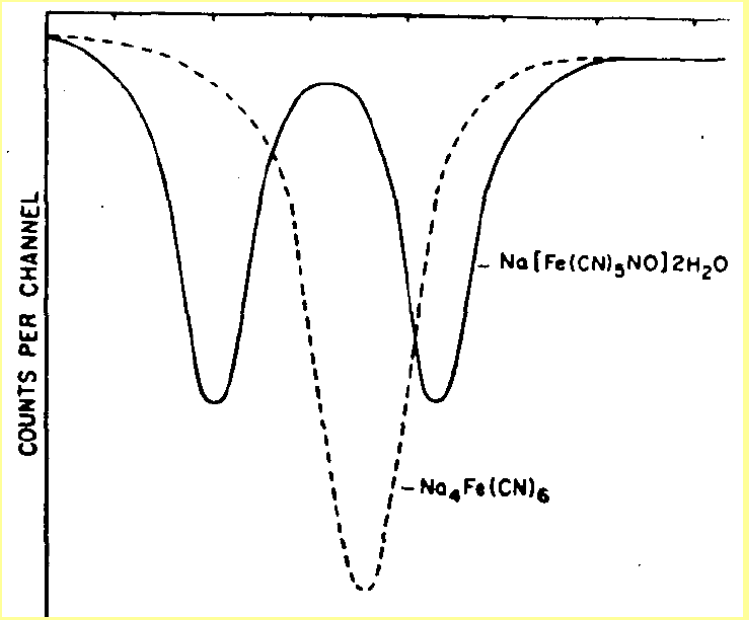

Unusually large ΔE_Q and too negative δ for Fe(II) LS (-0.165 mm/s)
NO withdraws electron density from d_{xz} a d_{yz} (π-bonding dp)

Isomer Shifts and Quadrupole Splitting

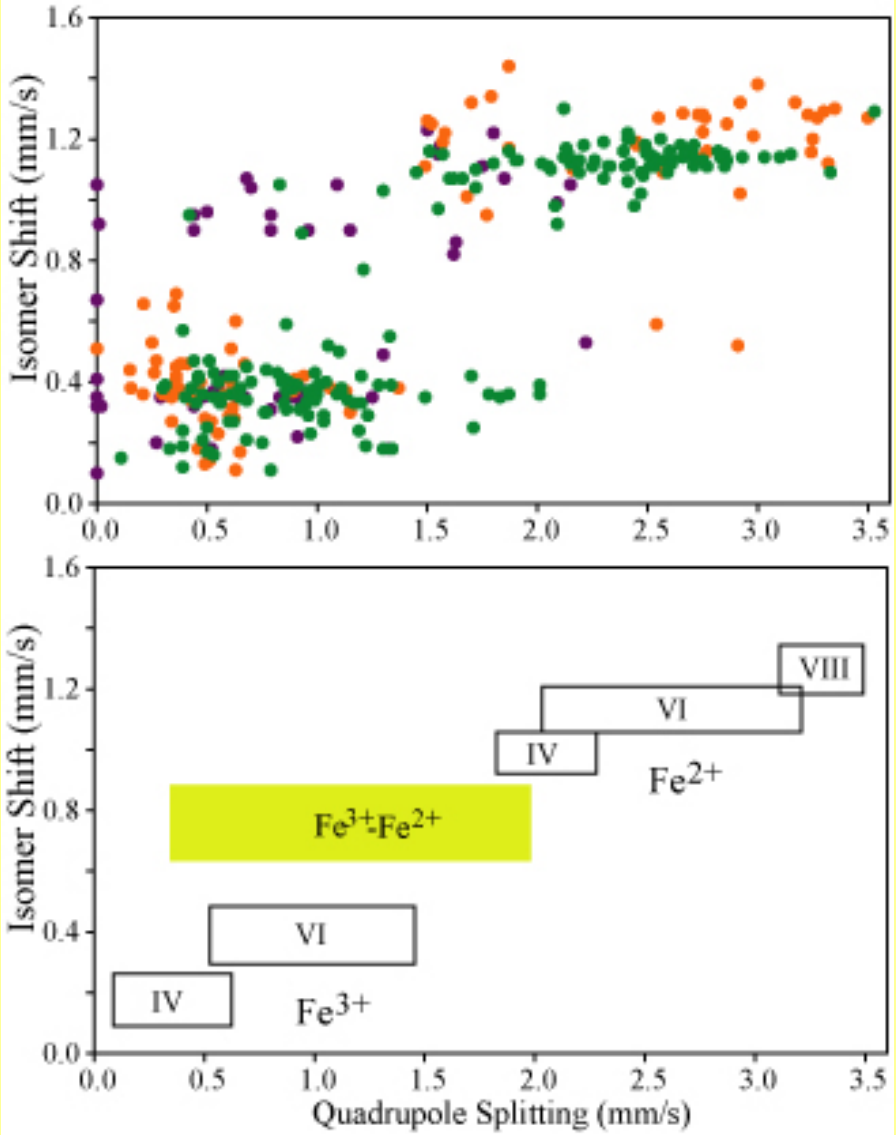

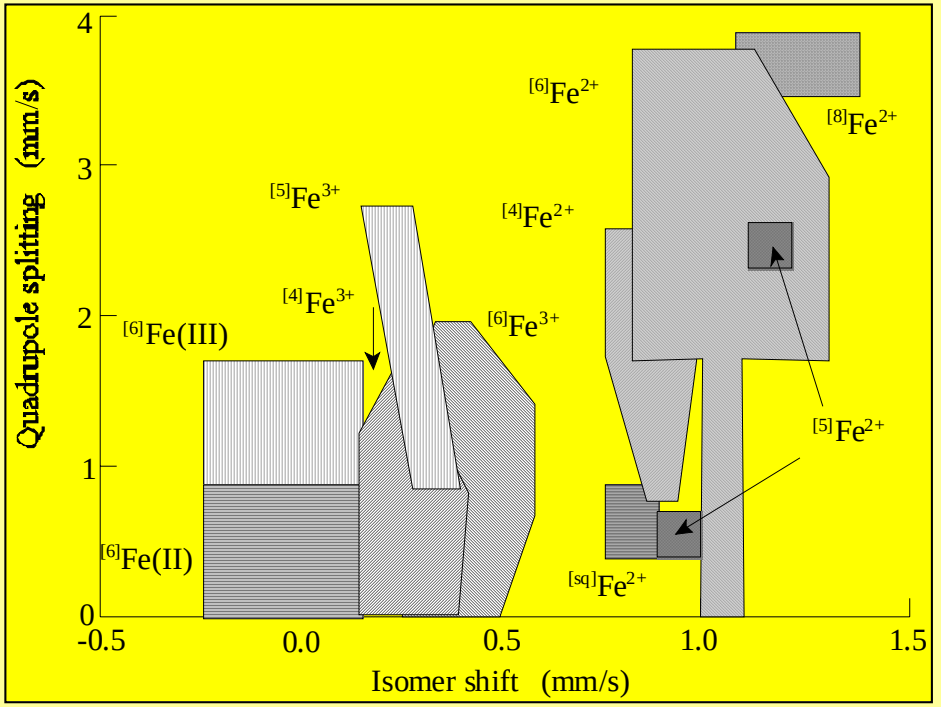

^{119}Sn Mössbauer Spectra and Structures of the Tin Halides

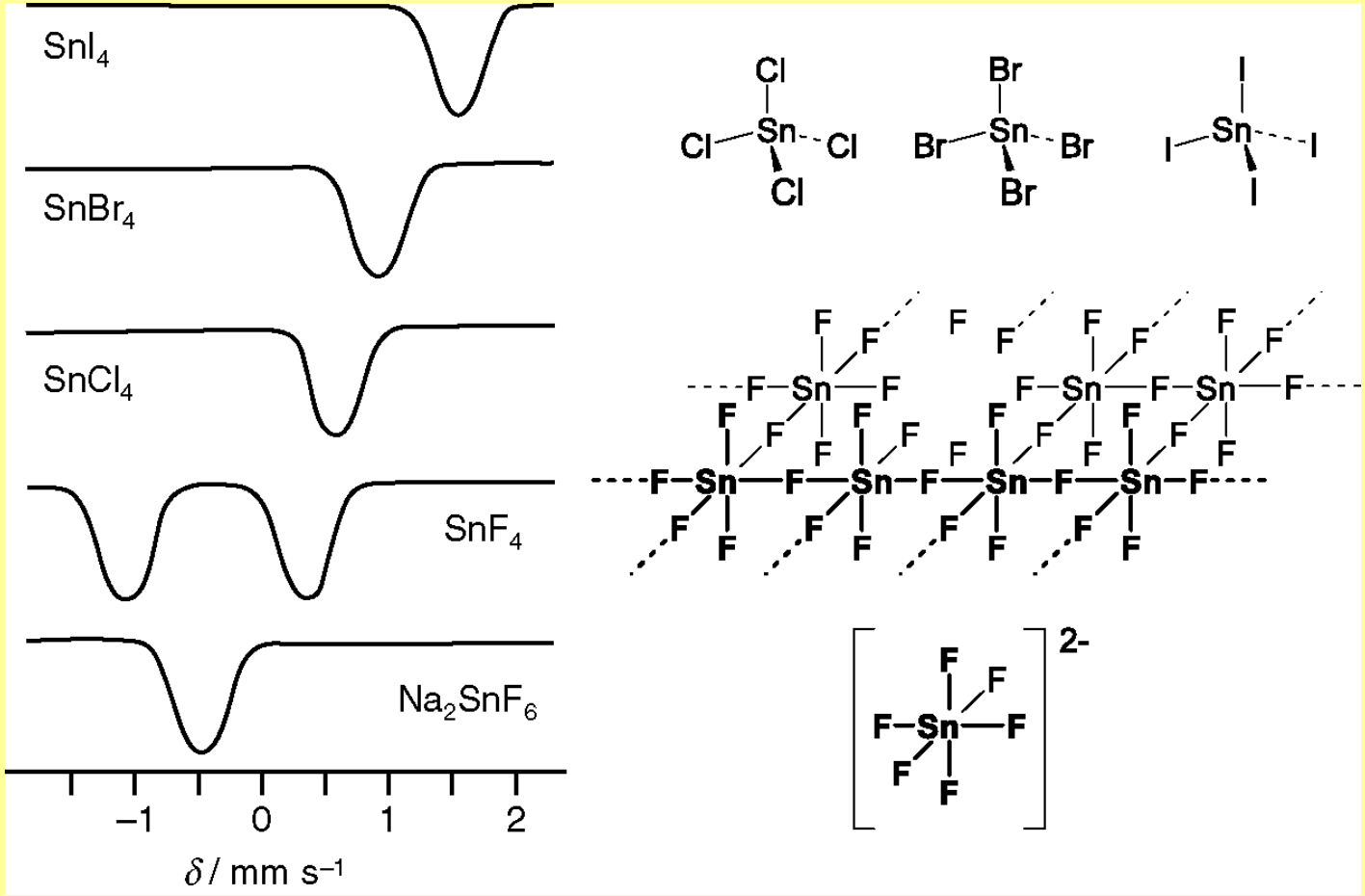

Magnetic Dipole Interaction

Magnetic Splitting ΔE_M

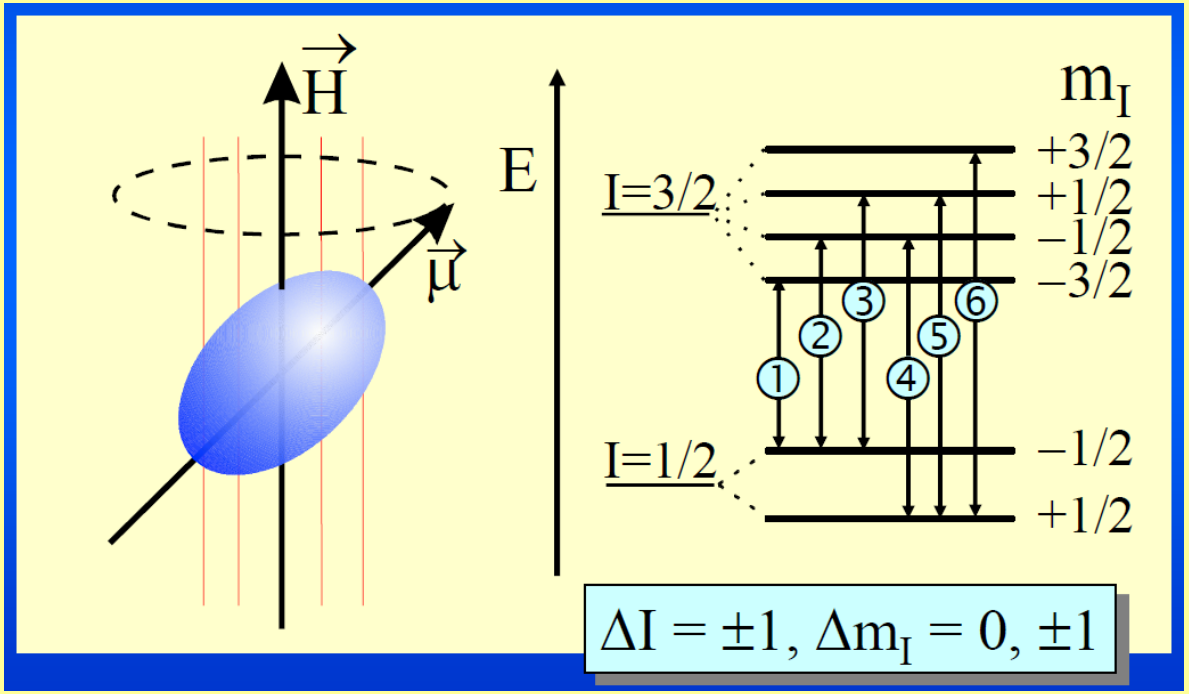

Magnetic dipole interaction = the precession of the magnetic dipole moment vector about the axis of the magnetic field

Splitting of the states I,m_I into $2I + 1$ substates

Magnetic Dipole Interaction

Magnetic Splitting ΔE_M

The requirements for magnetic dipole interaction
- the nuclear states involved possess a magnetic dipole moment μ ($I > ½$)
- a magnetic field is present at the nucleus

^{57}Fe: the ground state with $I = ½$ and the first excited state with $I = 3/2$

Selection rules: $\Delta I = \pm 1$, $\Delta m_I = 0, \pm 1$.

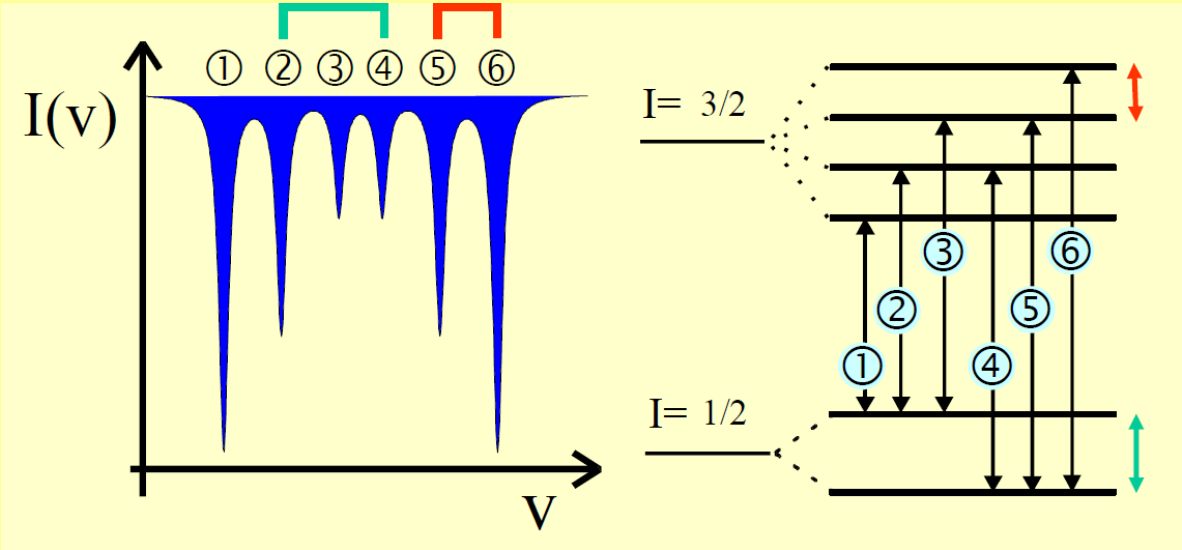

Magnetic Dipole Interaction

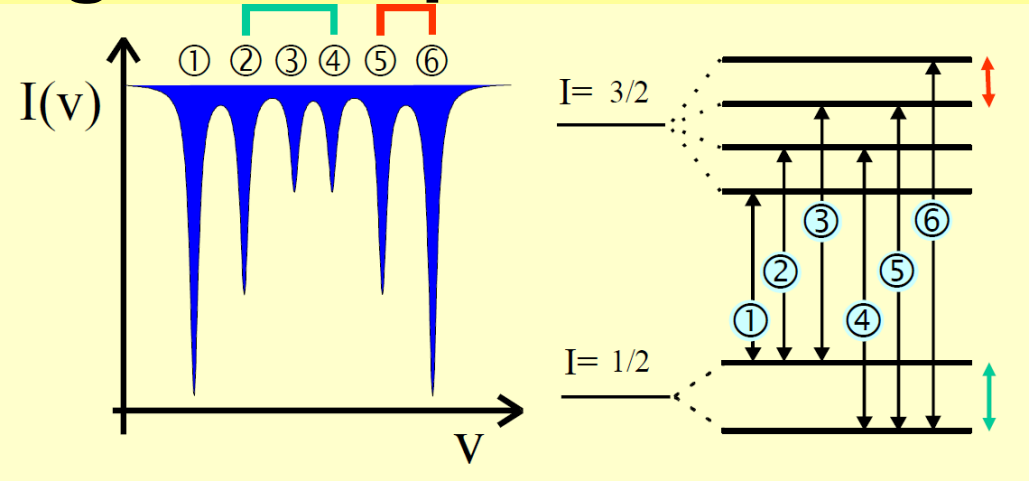

The energies of the sublevels :

$$E_M(m_I) = -\mu H m_I / I = -g_N \beta_N H m_I$$

g_N = the nulcear Landé factor, β_N = the nuclear Bohr magneton.

The separation between the lines 2 and 4 (also between 3 and 5) refers to the magnetic dipole splitting of the ground state.

The separation between lines 5 and 6 (also between 1 and 2, 2 and 3, 4 and 5) refers to the magnetic dipole splitting of the excited I = 3/2 state.

Internal Magnetic Field

A magnetic field H_{int} (r = 0) at the nucleus can originate in various ways:

$$\mathbf{H_{int} = H_C + H_D + H_L + H_{ext}}$$ = total internal magnetic field

Fermi Contact Interaction H_C:
Electron spin S of valence shell (e.g. S = 5/2 of Fe^{3+}) polarizes the s-electron density at the nucleus: **core polarisation**

Spin density $|\Psi(0)\downarrow|^2 > |\Psi(0)\uparrow|^2$ magnetic field $H_C \neq 0$

Spin dipolar interaction H_D:
The magnetic moment of the electron spin gives rise to dipolar interaction with the nucleus and causes a field at r = 0.

Internal Magnetic Field

Orbital dipolar interaction H_L:
Electrons with orbital moment L ≠ 0 give rise to an orbital magnetic moment accompanied by a magnetic field $\mathbf{H_L = -2\,\mu_B \langle r^{-3} \rangle \langle L \rangle}$

<L>: expectation value of orbital angular momentum.

Externally applied field H_{ext}:
By applying an external magnetic field of known size and direction one can determine the size and the direction of the intrinsic magnetic field of the material under investigation.

Combined Magnetic Dipole and Electric Quadrupole Interactions

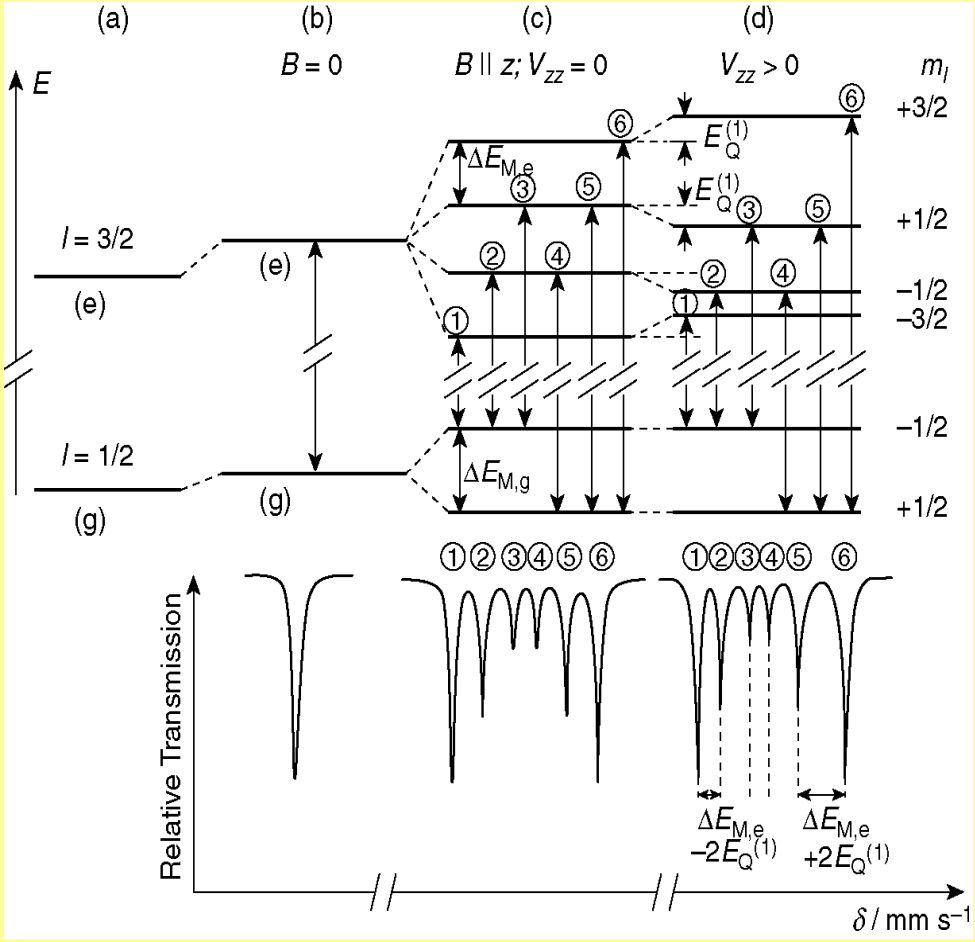

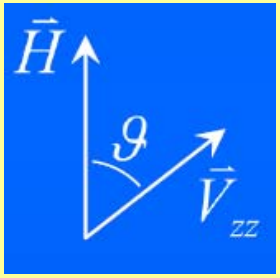

$$E_{M,Q}(I, m_I) = -g_N \beta_N H m_I + (-1)^{|m_I|+1/2} (eQV_{zz}/8)(3\cos^2 \vartheta - 1)$$

Combined Magnetic Dipole and Electric Quadrupole Interactions

Magnetic dipole interaction and electric quadrupole interaction may be present in a material simultaneously (together with the electric monopole interaction which is always present).

Relatively weak quadrupole interaction

The nuclear sublevels I,m_I arising from magnetic dipole splitting are additionally shifted by the quadrupole interaction energies $E_Q(I,m_I)$

The sublevels of the excited I = 3/2 state are no longer equally spaced. The shifts by E_Q are upwards or downwards depending on the direction of the EFG.

This enables one to determine the sign of the quadrupole splitting parameter ΔE_Q.

The quadrupole shift parameter ε depends on the canting angle φ of the spins with respect to the electric field gradient (*E*Q) axis [111]
$\varepsilon = \Delta E_Q(3\cos^2\varphi - 1)/2$ and thus yields values with opposite sign for AF ($\varphi = 0°$) and WF ($\varphi = 90°$) states.

Magnetic Dipole Interaction

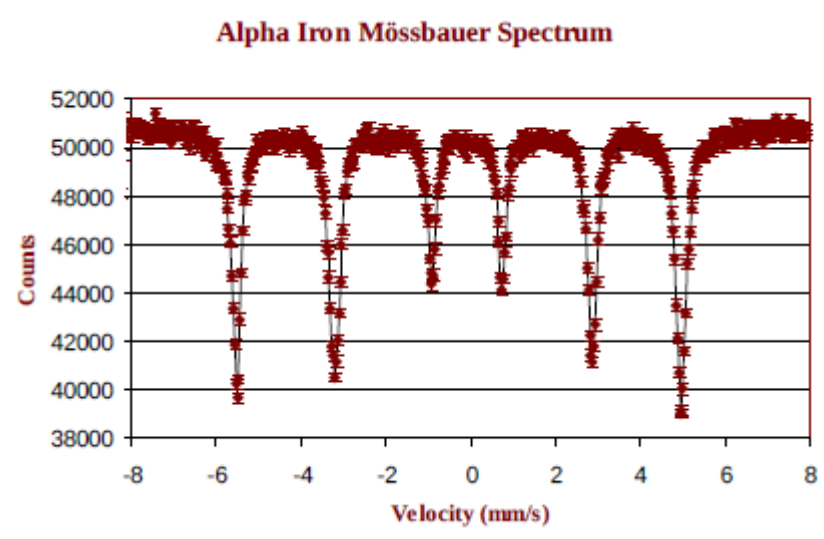

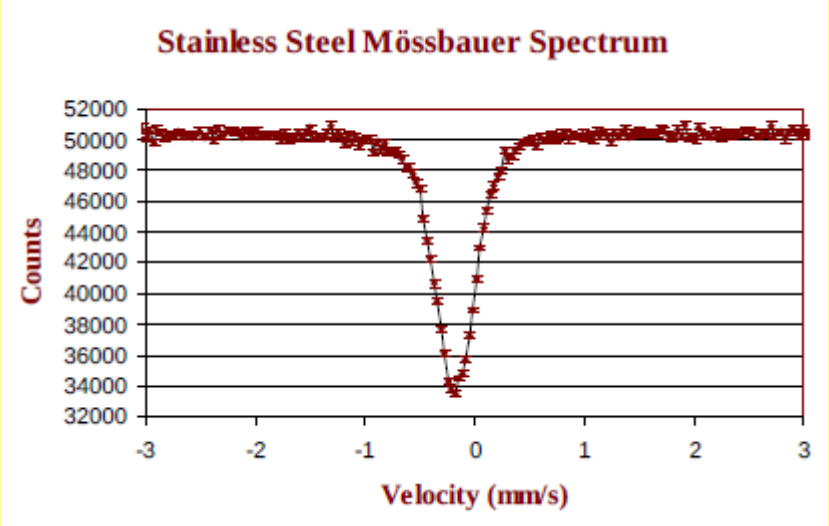

$Fe_3(CO)_{12}$

Possible Structures from X–Ray Diffraction

(Erickson, Fairhall 1965)

● Fe

○ CO

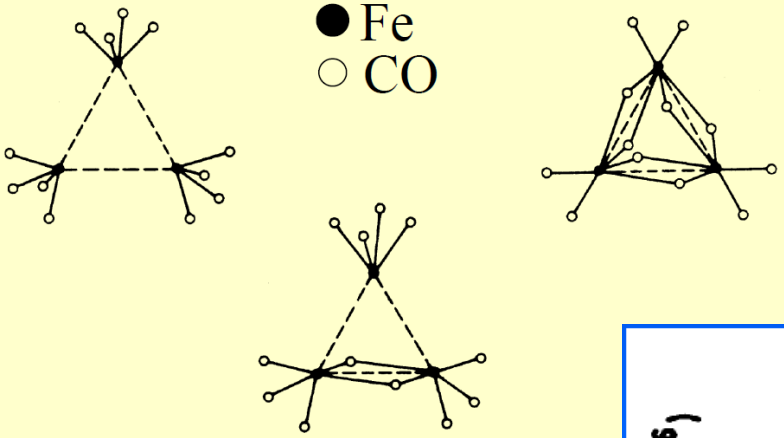

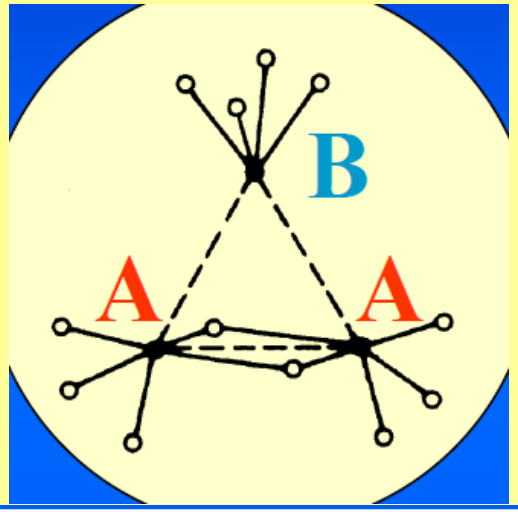

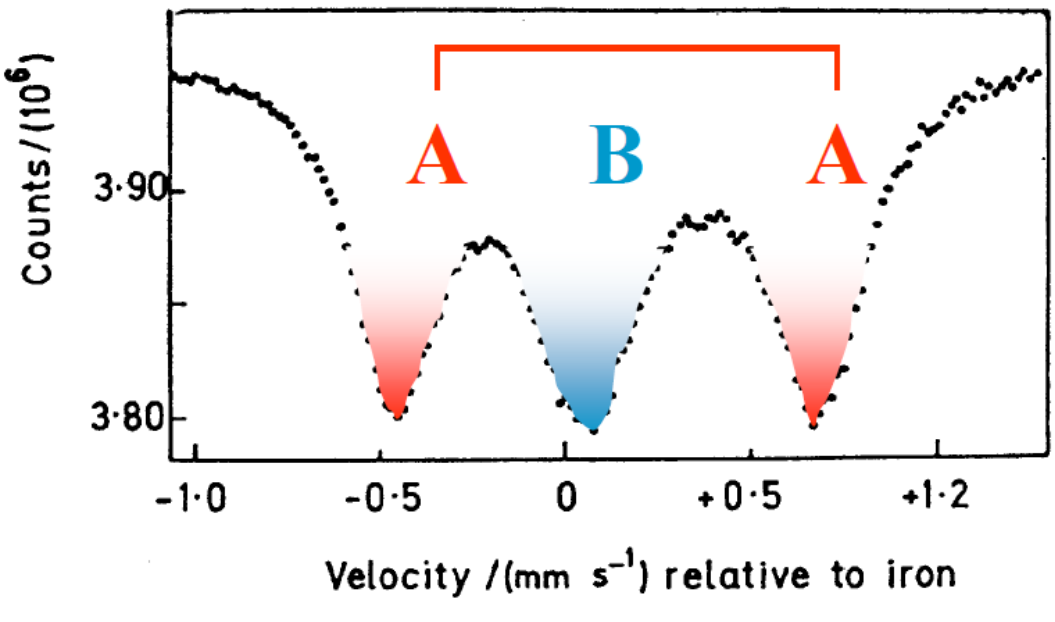

$[Fe_3(\mu_3\text{-}O)(OAc)_6(H_2O)_3]$

Variable-temperature ^{57}Fe Mössbauer spectra

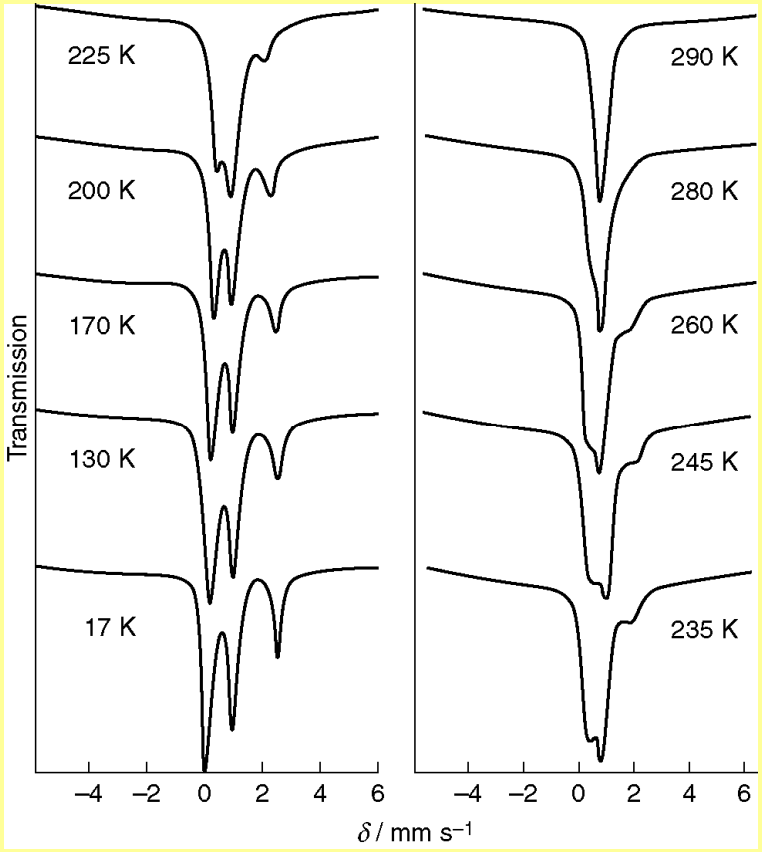

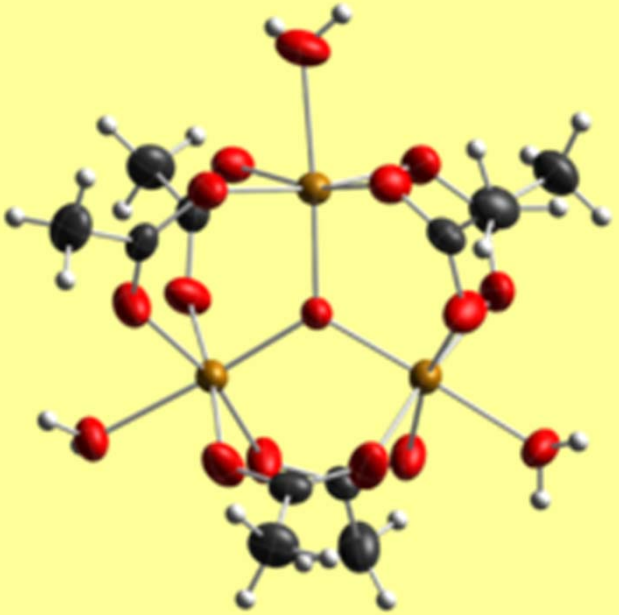

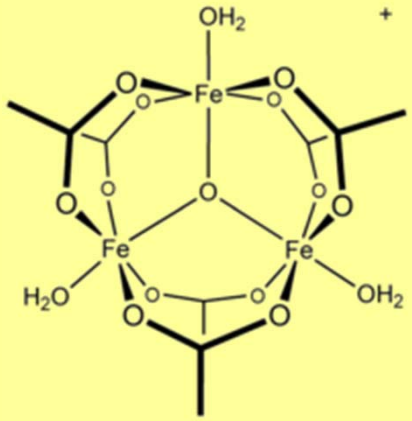

$[Fe_3(\mu_3\text{-}O)(OAc)_6(3\text{-}Et\text{-}py)_3]\bullet S$

Variable-temperature ^{57}Fe Mössbauer spectra

"$Fe^{2.67+}$"

Fe^{3+}-HS

Fe^{2+}-HS

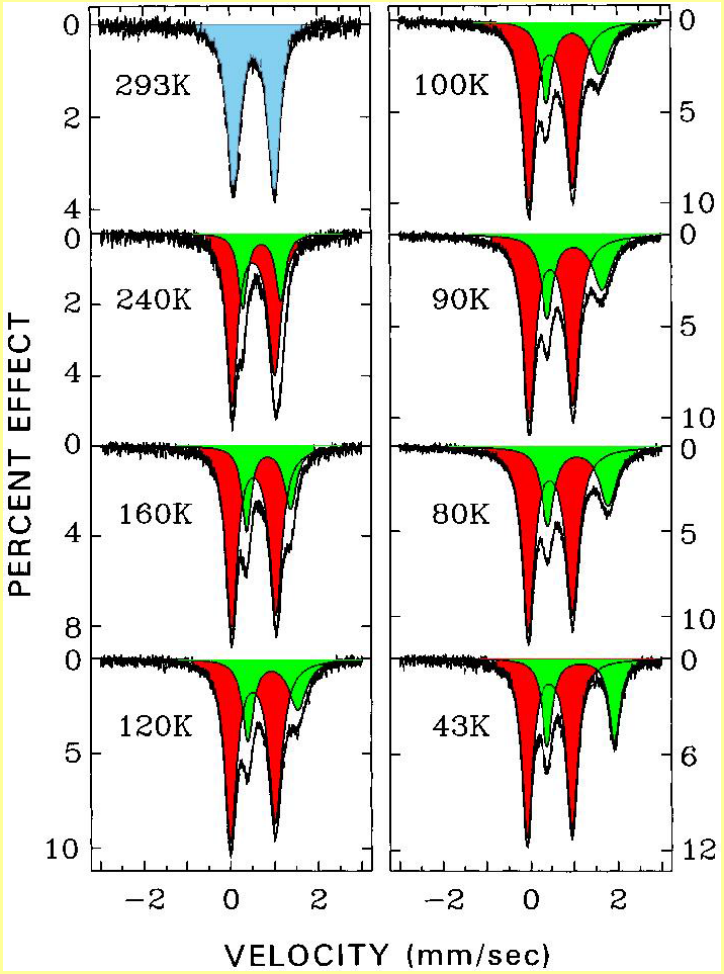

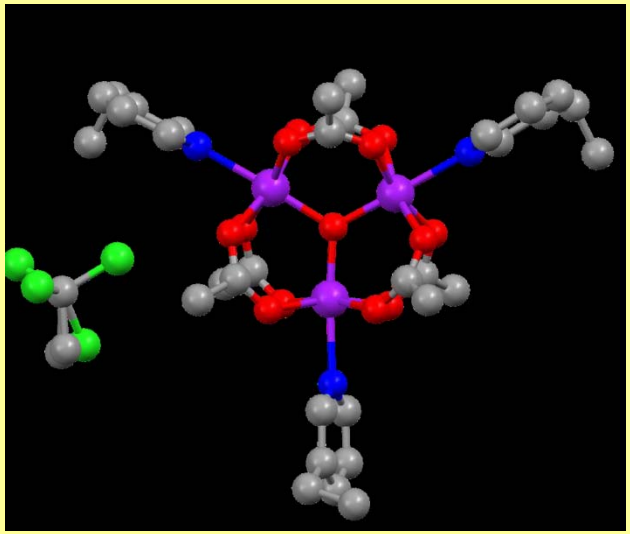

$S = CH_3CCl_3$

CH_3CCl_3 is valence-trapped at low temperature, increasing temperature leads to valence detrapping near room temperature. The ratio of the area fractions of Fe(III) to Fe(II) is close to 2 at low temperatures.

$[Fe_3(\mu_3\text{-}O)(OAc)_6(3\text{-}Et\text{-}py)_3]\bullet S$

Variable-temperature ^{57}Fe Mössbauer spectra

$S = C_6H_6 \quad CH_3CN$

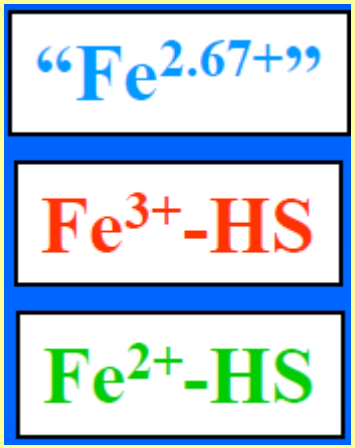

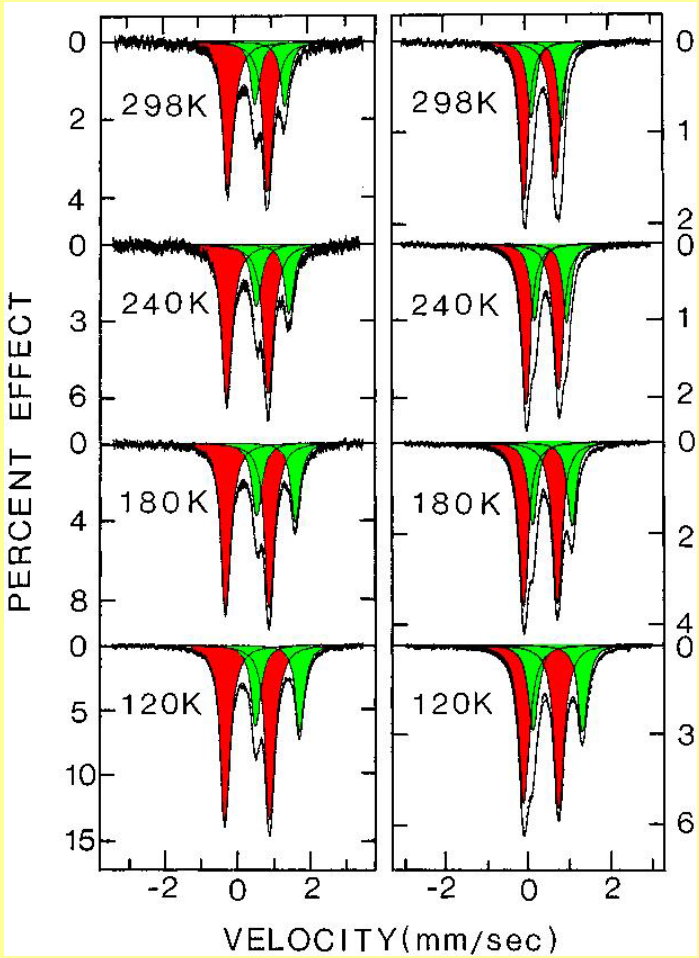

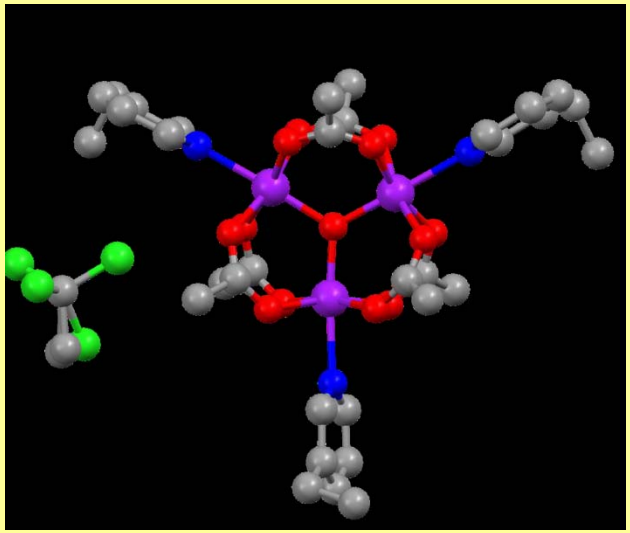

C_6H_6 is valence-trapped from 120 to 298 K on the Mössbauer time scale (given by the lifetime of the nuclear excited state).

CH_3CN increasing temperature leads to valence detrapping near room temperature.
The lattice packing controls valence de/trapping.
C_6H_6 possesses a stack type structure with strong intermolecular interactions due to overlapping pyridine ligands.
CH_3CN and CH_3CCl_3 are layered.

γ-Radiolysis of $FeSO_4 \cdot 7H_2O$ (300 K)

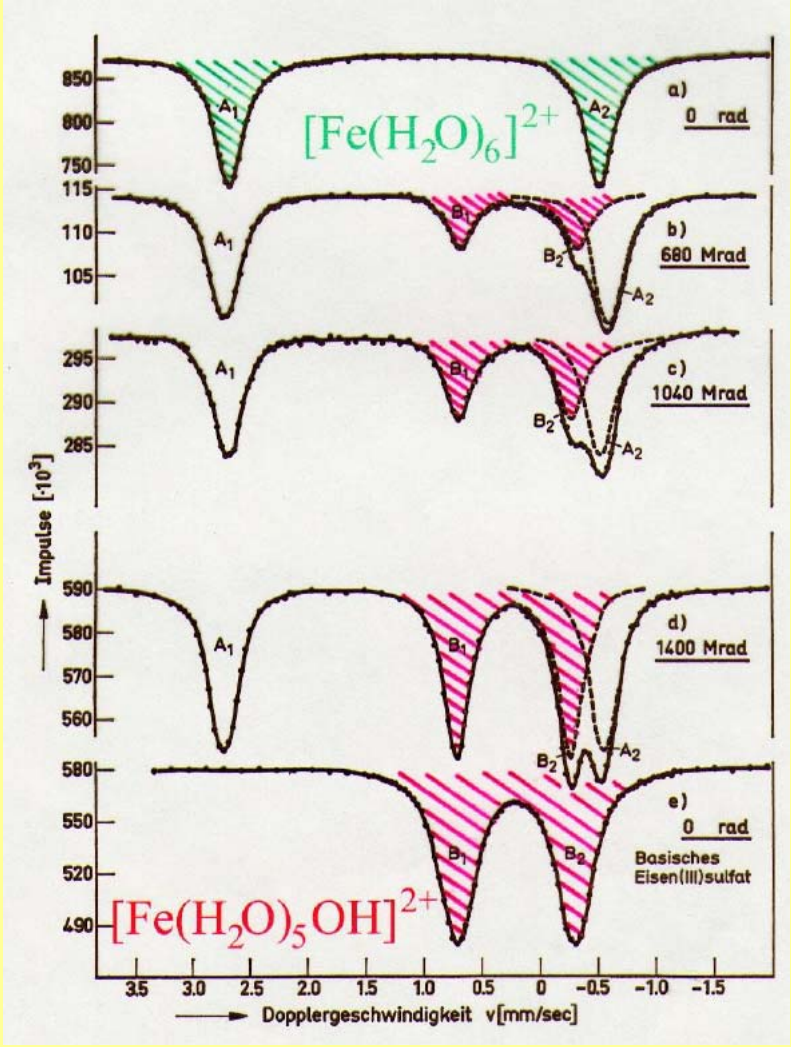

$$H_2O \rightsquigarrow H\bullet + \bullet OH$$

$$[Fe^{II}(H_2O)_5(\bullet OH)]^{2+} \rightarrow [Fe^{III}(H_2O)_5OH]^{2+}$$

Corrosion Products

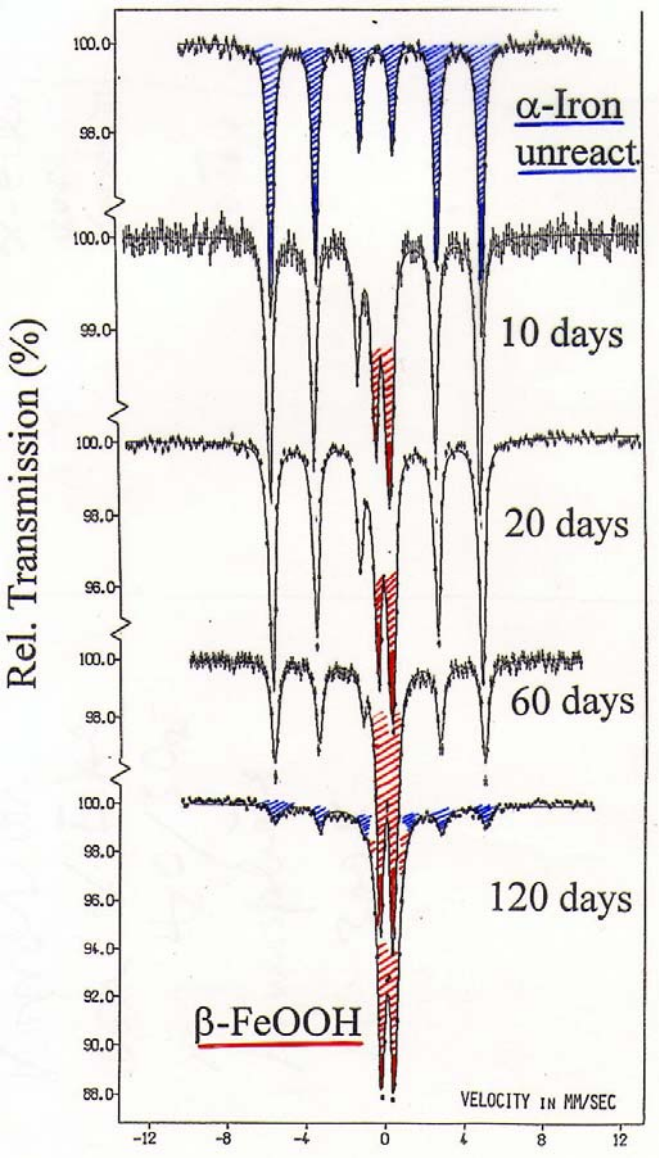

Corrosion of α-Iron
in H_2O/SO_2 atmosphere at 300 K

Corrosion product is β-FeOOH

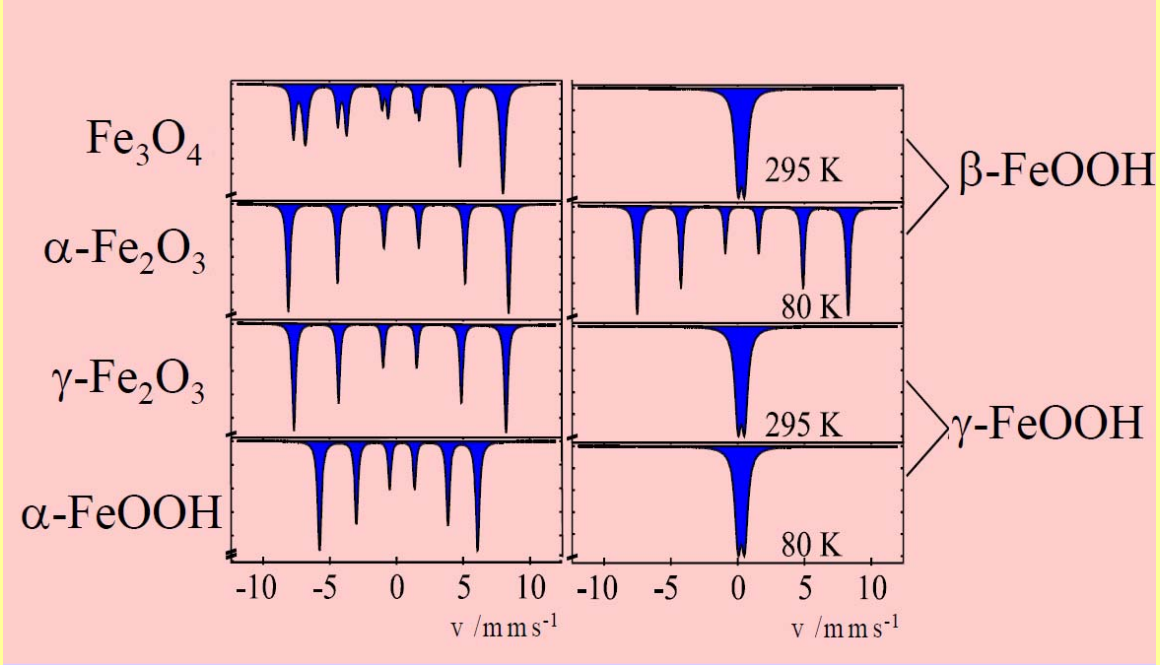

Iron(III) Oxides

iron(III) oxide phase	temperature [K]	Fe site	IS_{Fe} [mm/s]	QS/ε_Q [mm/s]	B [T]
α-Fe_2O_3	300		0.37	-0.21	51.7
	4.2		0.47	0.40	53.2
β-Fe_2O_3	300	d	0.37	0.69	-
		b	0.37	0.90	-
	15	d	0.50	0.23	47.9
		b	0.47	0.77	50.6
γ-Fe_2O_3	300	A	0.27	0	48.8
		B	0.41	0	49.9
	4.2	A	0.34	0	48.1
		B	0.49	0	51.0
ε-Fe_2O_3	300	Fe_1	0.37	-0.19	45.0
		Fe_2	0.39	-0.06	45.2
		Fe_3	0.38	0	39.5
		Fe_4	0.21	-0.07	26.3
amorphous-Fe_2O_3	300		0.34	0.78	-
	25		0.47	-0.03	46.8

IS_{Fe} – isomer shift related to metallic iron, QS – quadrupole splitting for doublet spectrum, ε_Q – quadrupole shift for sextet spectrum, B – hyperfine magnetic field

Iron(III) Oxides

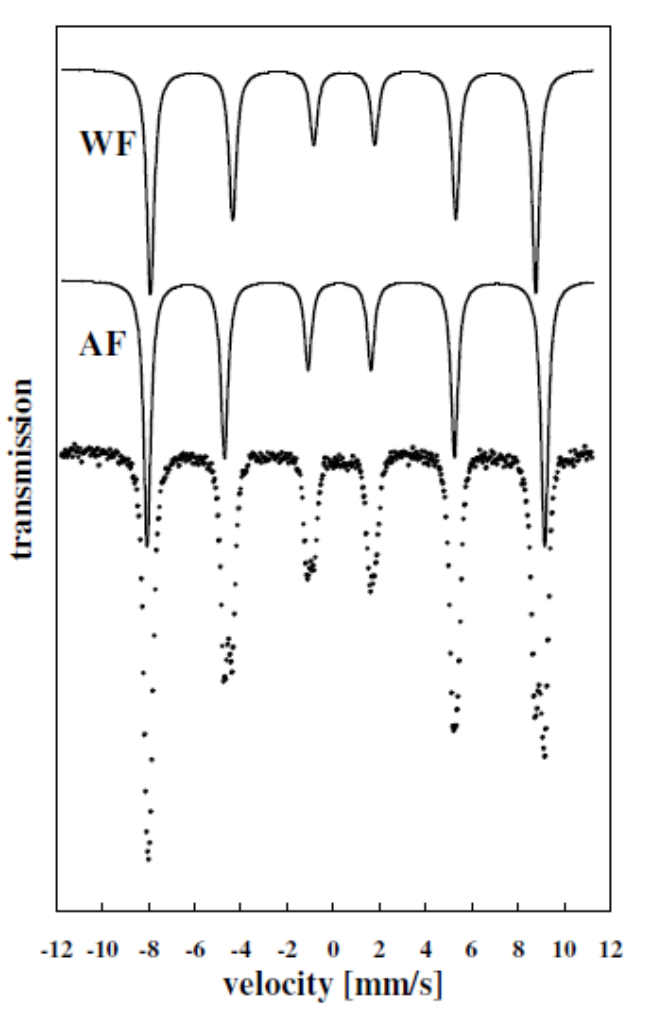

alpha-Fe_2O_3 measured at 260 K near Morin transition temperature

Hematite

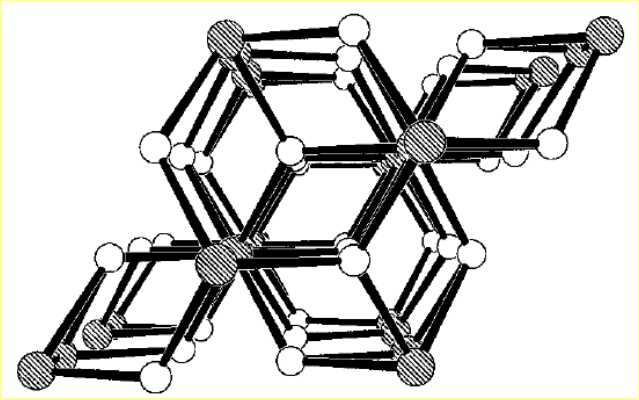

At < 260 K is antiferromagnetic (AF) with the spins oriented along the electric field gradient axis.

At Morin temperature (T_M), around 260 K, a reorientation of spins by about 90°, the spins become slightly canted to each other (by 5°), causing the destabilization of their perfect antiparallel arrangement = weak (parasitic) ferromagnetism between Morin and Neel temperature (T_N).

Above the Neel temperature of 950 K, hematite loses its magnetic ordering and is paramagnetic.

Iron(III) Oxides

Maghemite

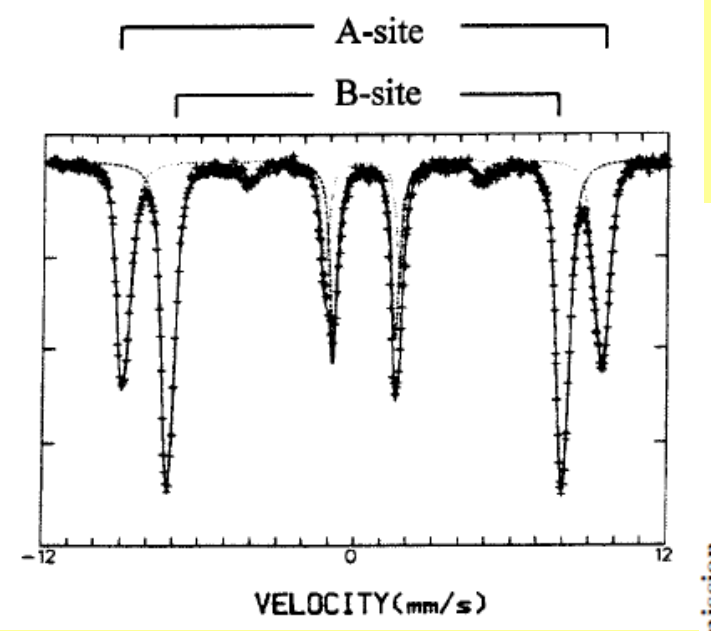

Mössbauer spectrum of a well-crystallized gamma-Fe_2O_3 at 4 K in an external field of 6 T.

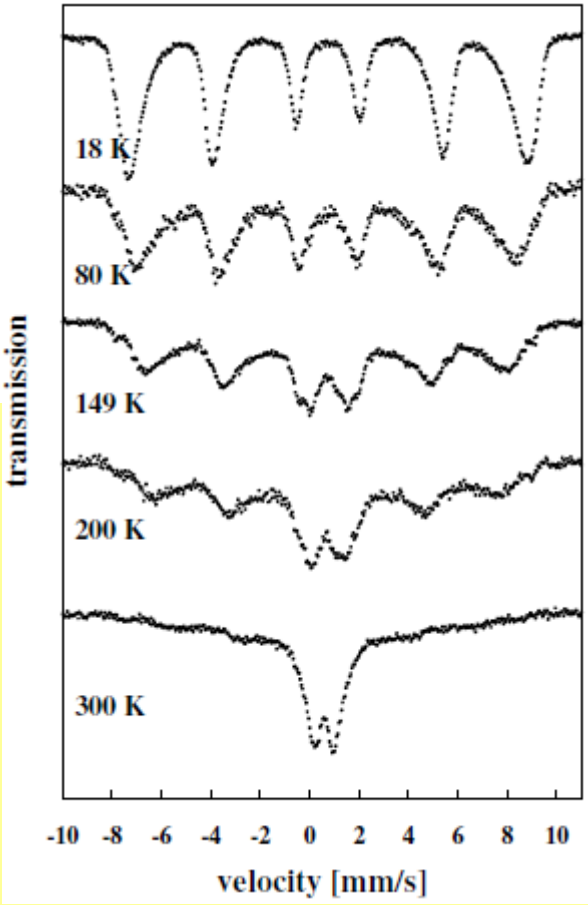

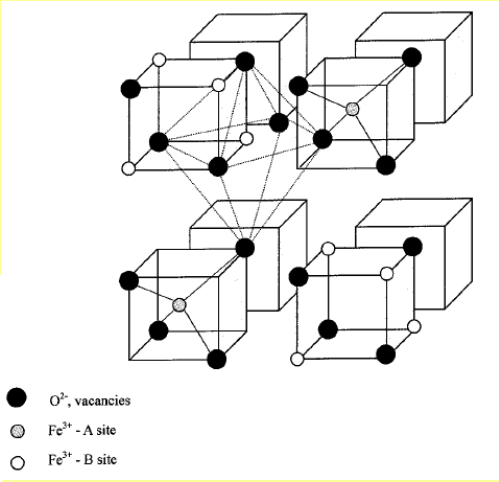

$$\left(Fe^{3+}\right)^{A}\left[Fe^{3+}_{5/3}\ \circ_{1/3}\right]^{B}O_4,$$

$$\left(Fe^{3+}_{8}\right)^{A}\left[\left(Fe^{3+}_{4/3}\ \circ_{8/3}\right)Fe^{3+}_{12}\right]^{B}O_{32},$$

Iron in French Red Wine